Structure

Article

Ca^{2+}-dependent lipid preferences shape synaptotagmin-1 C2A and C2B dynamics: Insights from experiments and simulations

Graphical abstract

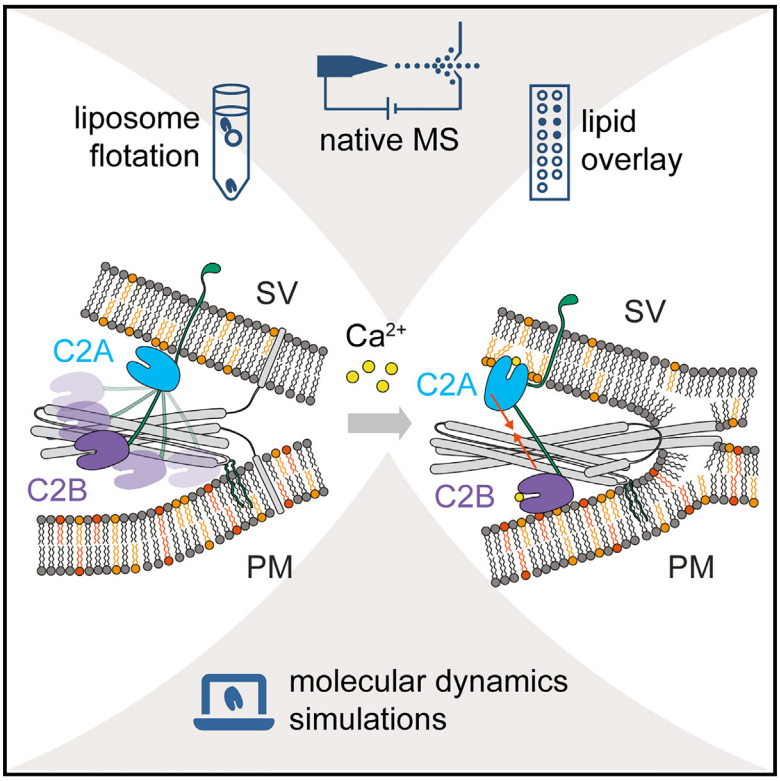

Highlights

- The C2A and C2B domains of synaptotagmin-1 interact with individual phospholipids
- Specific interactions of C2A and C2B with phospholipid membranes are Ca^{2+}-dependent
- C2A and C2B adopt a different orientation on phospholipid membranes
- A mechanism for synaptotagmin-1 during membrane fusion is proposed

Authors

Julian Bender, Til Kundlacz, Lucas S.P. Rudden, Melissa Frick, Julia Bieber, Matteo T. Degiacomi, Carla Schmidt

Correspondence

carla.schmidt@uni-mainz.de

In brief

The role of the calcium sensor synaptotagmin-1 during membrane fusion is still controversially discussed. Bender et al. follow a multidisciplinary approach and characterize lipid and membrane binding of its isolated C2 domains in the absence and presence of Ca^{2+}. Similarities and differences between the two domains are described.

Bender et al., 2024, Structure *32*, 1691–1704
October 3, 2024
https://doi.org/10.1016/j.str.2024.07.017

CellPress

Structure

CellPress
OPEN ACCESS

Article

Ca^{2+}-dependent lipid preferences shape synaptotagmin-1 C2A and C2B dynamics: Insights from experiments and simulations

Julian Bender,[1,5,7] Til Kundlacz,[1,2,7] Lucas S.P. Rudden,[3,6] Melissa Frick,[1] Julia Bieber,[4] Matteo T. Degiacomi,[3] and Carla Schmidt[1,4,8,*]

[1]Interdisciplinary Research Center HALOmem, Institute of Biochemistry and Biotechnology, Charles Tanford Protein Center, Martin Luther University Halle-Wittenberg, Kurt-Mothes-Straße 3a, 06120 Halle, Germany
[2]Institute of Chemistry, Martin Luther University Halle-Wittenberg, Von-Danckelmann-Platz 4, 06120 Halle, Germany
[3]Department of Physics, Durham University, South Road, Durham DH1 3LE, UK
[4]Department of Chemistry - Biochemistry, Johannes Gutenberg University Mainz, Hanns-Dieter-Hüsch-Weg 17, 55128 Mainz, Germany
[5]Present address: Chair of Biochemistry II, Theodor Boveri-Institute, University of Würzburg, Biocenter, Am Hubland, 97074 Würzburg, Germany
[6]Present address: Institute of Bioengineering, Swiss Federal Institute of Technology (EPFL), Lausanne 1015, Switzerland
[7]These authors contributed equally
[8]Lead contact
*Correspondence: carla.schmidt@uni-mainz.de
https://doi.org/10.1016/j.str.2024.07.017

SUMMARY

Signal transmission between neurons requires exocytosis of neurotransmitters from the lumen of synaptic vesicles into the synaptic cleft. Following an influx of Ca^{2+}, this process is facilitated by the Ca^{2+} sensor synaptotagmin-1. The underlying mechanisms involve electrostatic and hydrophobic interactions tuning the lipid preferences of the two C2 domains of synaptotagmin-1; however, the details are still controversially discussed. We, therefore, follow a multidisciplinary approach and characterize lipid and membrane binding of the isolated C2A and C2B domains. We first target interactions with individual lipid species, and then study interactions with model membranes of liposomes. Finally, we perform molecular dynamics simulations to unravel differences in membrane binding. We found that both C2 domains, as a response to Ca^{2+}, insert into the lipid membrane; however, C2A adopts a more perpendicular orientation while C2B remains parallel. These findings allow us to propose a mechanism for synaptotagmin-1 during membrane fusion.

INTRODUCTION

Signal transmission in neurons is accomplished by exocytosis of neurotransmitters from the lumen of synaptic vesicles into the synaptic cleft and subsequent binding of the neurotransmitters to neurotransmitter receptors at the postsynaptic membrane. To achieve this, a subset of synaptic vesicles docks at the presynaptic plasma membrane forming a pool of vesicles ready to fuse with the plasma membrane. Arrival of an action potential then causes influx of Ca^{2+} into the cytoplasm triggering membrane fusion.[1,2]

Docking of the vesicles and fusion of the vesicle and plasma membranes requires formation of the SNARE (i.e., soluble N-ethylmaleimide-sensitive-factor attachment receptor) complex, the neuronal membrane fusion machinery.[3] The SNARE complex assembles from three SNARE proteins, namely synaptobrevin-2, SNAP25, and syntaxin-1A, by formation of a tight four-helix bundle.[4–6] Zippering of the helices proceeds from their N-termini toward their C-termini through interactions of their SNARE motifs.[7,8] As a result, the two lipid bilayers are pulled together resulting in fusion of the membranes. Formation of the SNARE complex and fusion of the membranes is regulated by various proteins including, for instance, the complexins[9,10] or synaptotagmin-1, the primary Ca^{2+} sensor of synaptic vesicles.[11]

Synaptotagmin-1 contains a short luminal domain, an α-helical transmembrane anchor, as well as two cytosolic C2 domains (i.e., C2A and C2B) connected through flexible linkers.[12,13] The C2A and C2B domains form β-sandwich structures accommodating aspartate-containing Ca^{2+} binding loops that coordinate three (C2A) and two (C2B) Ca^{2+} ions.[14–17] C2B contains an additional polybasic region close to the Ca^{2+} binding loops.[14] Ca^{2+} binding alters the electrostatic surface potential of synaptotagmin-1 resulting in membrane binding of the C2 domains through the head groups of anionic phospholipids.[18,19] Ca^{2+}-dependent interactions with the membrane are further mediated by penetration of the C2 domains into the hydrophobic core of the lipid membrane[20,21] as well as electrostatic interactions of the polybasic stretch and two arginine residues with multivalent phosphoinositides.[22–24] Likewise, an increase in membrane affinity upon Ca^{2+} binding was reported.[25–27]

Recently, the membrane binding characteristics of the C2A and C2B domains were described as follows: C2A does not bind membranes containing phosphatidylserine (PS) or phosphatidylinositide in the absence of Ca^{2+}. In the presence of Ca^{2+}, C2A preferably binds PS-containing membranes. C2B, on the other hand, preferentially binds to and inserts into membranes containing phosphatidylinositol 4,5 bisphosphate ($PI(4,5)P_2$).[28] Therefore, a "bridging" mechanism of synaptotagmin-1 implying a preference of C2A for the *cis* membrane, i.e., the membrane it is anchored to, and of C2B for the target *trans* membrane was reasoned.[28]

Even though the general function of synaptotagmin-1 is well understood, the exact working principle is still controversially discussed.[29] This includes, among other aspects, the lipid preferences of the two C2 domains that govern membrane binding. We, therefore, follow a multidisciplinary approach and study interactions of C2A and C2B with specific lipids and lipid membranes of defined composition in the absence and in the presence of Ca^{2+}. Specifically, we characterize binding of specific lipid classes by lipid overlay assays and native mass spectrometry and then explore association of the C2A and C2B domains to lipid bilayers in liposome flotation assays. We found that both C2 domains bind a variety of individual lipids; in solution, these interactions were enhanced in the presence of Ca^{2+}, while interactions that were captured in the gas phase occurred independently of Ca^{2+} binding. Importantly, the C2A and C2B domains require Ca^{2+} to associate with a phospholipid bilayer of specific composition. Finally, we make use of molecular dynamics simulations of C2A and C2B in the presence of model membranes resembling the vesicle and plasma membranes to gain detailed insight on the structural dynamics, lipid contacts, membrane penetration and contact angles of synaptotagmin-1. Our simulations unravel differences between the C2A and C2B domains in their membrane orientation and insertion depth, allowing us to provide a mechanistic model for membrane fusion facilitated by synaptotagmin-1.

RESULTS

C2A and C2B preferably bind negatively charged phospholipids

To study lipid and membrane binding of the individual C2 domains of synaptotagmin-1, we chose two variants including the sequences of the individual C2A and C2B domains, respectively, as well as parts of the N-terminal (C2A) and C-terminal (C2B) linkers (Figure 1A). Both proteins were purified through an affinity strategy using an N-terminal His-tag (see STAR Methods for details). Following purification, the His-tag was cleaved with thrombin as confirmed by gel electrophoresis showing a mass difference of approximately 1 kDa between the tagged and the untagged protein (Figure 1B). The molecular weight of the C2A and C2B domains was then confirmed by native mass spectrometry revealing charge state distributions corresponding in mass to 19.5 kDa (C2A) and 17.6 kDa (C2B), respectively (Figure 1B).

As lipid binding depends on the correct folding of the C2 domains, we analyzed their secondary structure by far-UV circular dichroism (CD) spectroscopy and compared experimentally observed with theoretically calculated CD spectra (STAR Methods). The spectra of C2A and C2B both showed a local minimum at 218 nm, which is characteristic for the anti-parallel β-sheet structure of the C2A and C2B domains (Figure 1C).

Having confirmed formation of secondary structure elements of the C2A and C2B domains comparable to existing high-resolution structures, we next explored their binding specificity for the head groups of specific lipid classes. For this, membrane lipid strips spotted with 100 pmol of different lipids were incubated with C2A and C2B in the absence or in the presence of Ca^{2+} and bound protein was detected using specific primary and secondary antibodies. To mimic native conditions, we either removed free Ca^{2+} ions by addition of 1 mM EGTA providing a Ca^{2+}-free environment similar to the pre-fusion state or we added 500 μM $CaCl_2$ representing a high Ca^{2+} concentration as observed during an action potential. Note that the intracellular Ca^{2+} concentration increases locally approximately thousand-fold during an action potential (reaching up to 300 μM[30]); we compensate for this by adding 500 μM in these *in vitro* experiments. In the absence of Ca^{2+}, C2A and C2B specifically bound phosphatidylinositol phosphate (PI(4)P), phosphatidic acid (PA) and, at very low intensities, sulfatides (Figure 2A). C2B further showed weak binding to PS and strong binding to cardiolipin. In the presence of Ca^{2+}, binding to PI(4)P significantly increased and binding to phosphatidylinositol bisphosphate ($PI(4,5)P_2$; C2A and C2B domains) and phosphatidylinositol trisphosphate ($PI(3,4,5)P_3$; only C2B domain) was observed in addition to the previously detected lipids (Figure 2A). These binding assays confirm that Ca^{2+} indeed affects the interactions of synaptotagmin-1 with phosphatidylinositol phosphates.

We then explored interactions of C2A and C2B with different lipids in solution following a strategy presented recently.[31] For this, mixed detergent-lipid micelles serve as vehicles of lipids in solution during electrospray ionization for native mass spectrometry, transferring lipids onto the protein surface upon contacts with the micelle in the electrospray droplet.[31] To achieve this, we incubated the C2A and C2B domains with mixed detergent-lipid micelles and subsequently analyzed the protein-lipid complexes that formed by native mass spectrometry (Figure 2B). We first explored lipid transfer of negatively charged dioleoyl (DO) phospholipids including DOPS, DOPI, DOPI(4)P, $DOPI(4,5)P_2$ and $DOPI(3,4,5)P_3$ (Figures 2B and S1). As expected, binding of all lipids was observed, and intensities of protein-lipid complexes increased at higher concentration of the lipids. Native mass spectra further reveal binding of up to three lipids per C2 domain. In agreement with the observed specificity for negatively charged lipids (see previous text), highest intensities were observed for $DOPI(3,4,5)P_3$ (Figure S1). In addition to negatively charged phospholipids, we also explored binding of zwitterionic DOPC. Again, binding of up to three lipid molecules was observed at high lipid concentration (Figure S1); we assume that electrostatic interactions between the positively charged choline head group and negatively charged Ca^{2+}-binding loops are stabilized in the gas-phase during native mass spectrometry experiments.[32] Importantly, increasing the collisional voltage in the collision cell of the mass spectrometer to only 30 V caused dissociation of DOPC, while $DOPI(4,5)P_2$ remained stably associated with C2B even at a collisional voltage of 60 V (Figure S2). Presumably, electrostatic interactions between the positively charged residues of the C2 domains and negatively charged $DOPI(4,5)P_2$ are stronger than

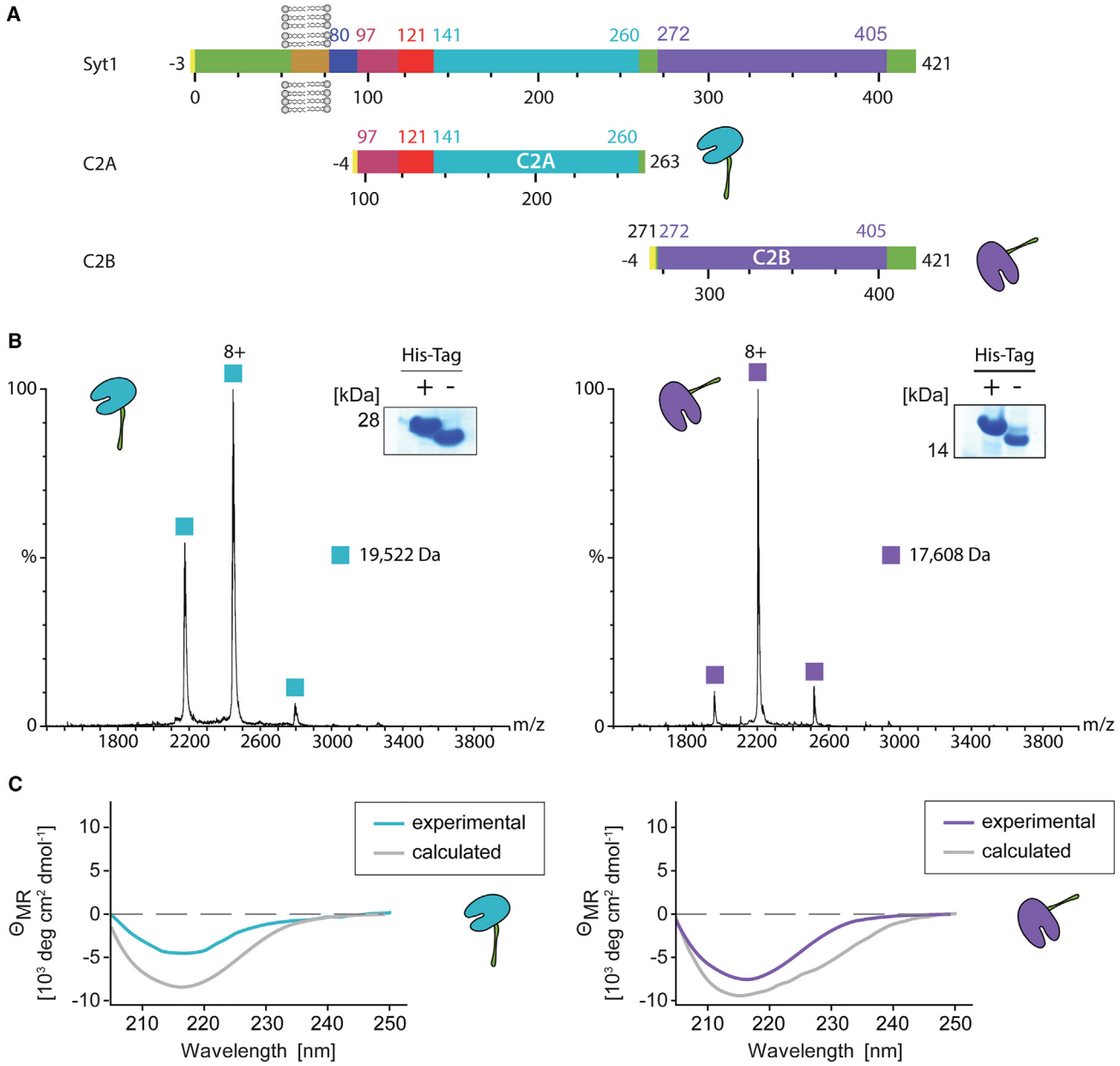

Figure 1. Purified C2A and C2B domains

(A) Schematic of full-length synaptotagmin-1 (Syt1) as well as the C2A (cyan) and C2B (purple) constructs used in this study.

(B) Native mass spectrometry of C2A (cyan) and C2B (purple). Successful cleavage of the His-tag was verified by gel electrophoresis (inserts).

(C) Far-UV CD spectroscopy of C2A (cyan) and C2B (purple) domains confirmed β-sheet formation of the purified proteins. Experimentally determined CD spectra (cyan, purple) are compared to calculated, theoretical spectra (gray).

those between the negatively charged Ca^{2+}-binding loops and zwitterionic DOPC.

As reported previously, synaptotagmin-1 binds phospholipids in the presence and in the absence of Ca^{2+}, and importantly, Ca^{2+} and phospholipid binding modulate the strength of these interactions cooperatively.[22–24] We, therefore, compared phospholipid binding to the C2A and C2B domains in the presence and in the absence of Ca^{2+}. For this, the proteins were pre-incubated with Ca^{2+} or EGTA (to mimic the Ca^{2+}-free state) and phospholipids were transferred to the domains as described (see previous text). The analysis of proteins by native mass spectrometry in the presence of high salt concentrations is not trivial, and instrument conditions were adjusted carefully (method details). First, Ca^{2+} binding was confirmed for the two domains in the absence of phospholipids. Indeed, as reported previously,[14–17] binding of three or two Ca^{2+} ions was observed for the C2A and C2B domains, respectively (Figure S3). We then compared lipid binding to the C2 domains in the presence of

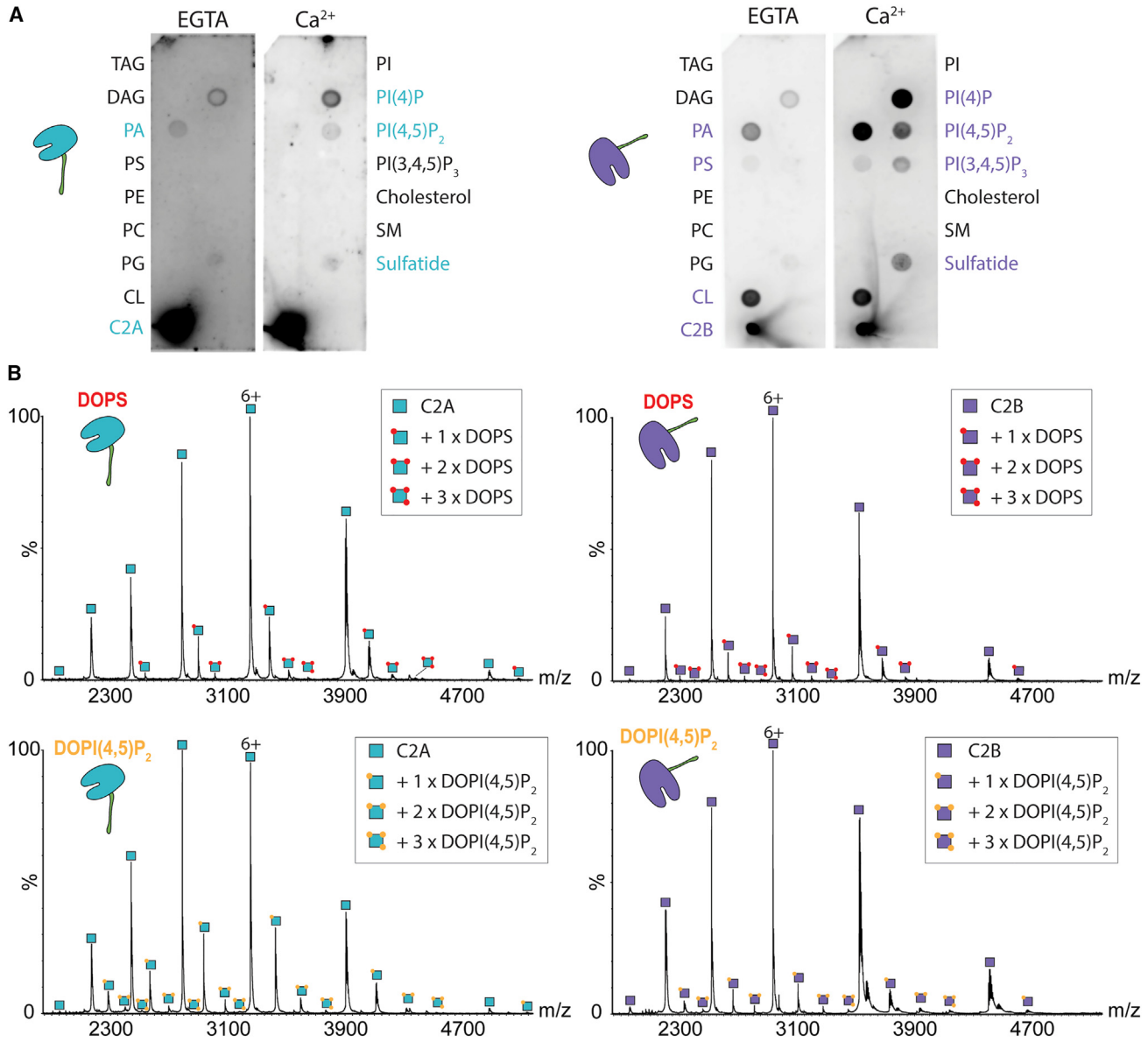

Figure 2. C2A and C2B domains bind negatively charged phospholipids

(A) Lipid overlay assays. Membrane lipid strips spotted with different membrane lipids were incubated with C2A (lhs, cyan) and C2B (rhs, purple). Protein binding was visualized using specific antibodies.

(B) Native mass spectrometry reveals binding of C2A (lhs, cyan) and C2B (rhs, purple) to up to three DOPS (red) and DOPI(4,5)P_2 (yellow) molecules.

See also Figures S1 and S2.

EGTA or Ca^{2+}. We specifically focused on two negatively charged phospholipids, namely DOPS and DOPI(4,5)P_2, as well as zwitterionic DOPC. Native mass spectra revealed lipid adducts for all phospholipids in the absence and in the presence of Ca^{2+} (Figure S4). As the analysis of the proteins in the presence of Ca^{2+} required higher collisional voltages (method details), lipid adducts partially dissociated resulting in loss of lipid adducts from higher charge states as well as lower intensities of the protein-lipid complexes in general. Nonetheless, interactions of C2A and C2B with all phospholipids were observed, independent on the presence of Ca^{2+} or EGTA. Interestingly, we again found lipid adducts of zwitterionic DOPC albeit at low intensity and only with low charge states. In addition, DOPC easily dissociates from the protein-lipid complexes (Figure S4A) confirming that interactions in the gas phase are weaker with DOPC than with negatively charged lipids. We reason that both C2 domains interact with mixed detergent-lipid micelles independently of Ca^{2+} binding, and that these interactions are captured during ionization when the proteins are transferred into the gas phase.

Ca^{2+} affects membrane binding of C2A and C2B

Having explored lipid binding to the C2 domains of synaptotagmin-1 in solution through contacts with detergent-lipid

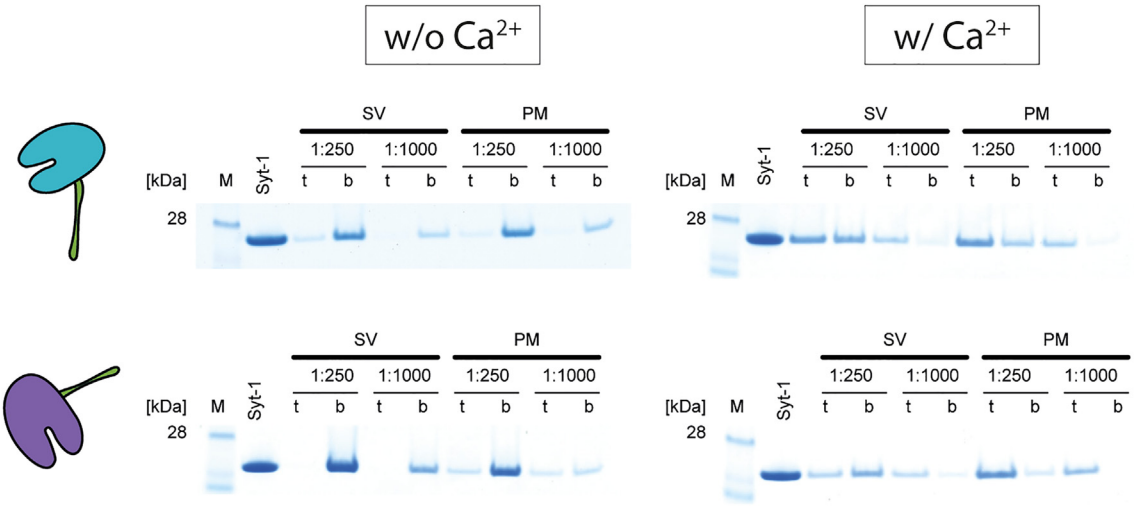

Figure 3. Binding of C2A and C2B to phospholipid bilayers is affected by Ca^{2+}

C2A (cyan) and C2B (purple) were incubated with liposomes resembling the synaptic vesicle membrane (SV) or the presynaptic plasma membrane (PM). Binding to the liposome membranes was then analyzed by liposome flotation on a sucrose gradient. Top (t) and bottom (b) fractions were collected, and protein binding was monitored by gel electrophoresis.

micelles and immobilized lipids, we next explored binding of C2A and C2B to phospholipid bilayers. For this, we made use of liposomes of different composition resembling the synaptic vesicle membrane and the presynaptic plasma membrane, respectively.[33] Accordingly, liposomes containing DOPC:DOPS:DOPE:cholesterol at a molar ratio of 38:12:20:20 (synaptic vesicle membrane) or DOPC:DOPS:DOPE:PI(4,5)P_2:DAG:cholesterol at a molar ratio of 38:12:20:2:2:20 (presynaptic plasma membrane; DAG, diacylglycerol) were prepared as described (see method details). The C2A and C2B domains were then incubated with the liposomes and, subsequently, overlaid with a sucrose gradient. After centrifugation, top and bottom fractions of the gradient were collected and analyzed by gel electrophoresis for their protein content. Proteins that associate with the liposome membrane will be identified in the top fractions together with the liposomes, which float on the sucrose gradient. Proteins that do not bind the liposome membrane ("free protein") will be identified in the bottom fractions.

We compared binding of the C2A and C2B domains to liposomes resembling the synaptic vesicle and the presynaptic plasma membranes in the absence and in the presence of Ca^{2+} at two protein:lipid ratios (1:250 and 1:1,000). In the absence of Ca^{2+}, C2A and C2B were mostly identified in the bottom fractions and only a small proportion of both domains was observed in the top fractions when using liposomes that were composed of the presynaptic plasma membrane lipid mixture (Figure 3). However, when performing these experiments in the presence of Ca^{2+}, the majority of both proteins were identified in the top fractions, i.e., both domains associated with the liposome membranes in the presence of Ca^{2+}. These effects were most prevalent for the C2B domain, binding liposomes that resemble the presynaptic plasma membrane. In addition, binding of C2A to synaptic vesicle and plasma membrane liposomes as well as binding of C2B to synaptic vesicle liposomes was also observed, albeit at lower intensity. When comparing the two protein:lipid ratios, we did not observe major differences; however, the results were more distinct when using a higher protein:lipid ratio (i.e., 1:1,000).

In summary, we found that Ca^{2+} affects the binding of the C2A and C2B domains to phospholipid membranes. While both domains appear to associate in the presence of Ca^{2+} with the two membrane compositions employed here, C2B appears to be particularly selective to the presynaptic plasma membrane mimetic.

Molecular dynamics simulations assess structural flexibility of C2A and C2B

To advance our *in vitro* findings and develop a model elucidating the molecular details of C2 lipid-preferences, we simulated the interactions of C2A and C2B with model membranes corresponding to the synaptic vesicle and the plasma membrane in the presence and in the absence of Ca^{2+}. Briefly, we extracted the structures of Ca^{2+}-bound C2A and C2B from an available high-resolution structure of Synaptotagmin-1 C2AB (PDB: 5KJ7 [34]) and removed the Ca^{2+} ions to generate Ca^{2+}-free structures (see STAR Methods for details). The initial lipid membrane model was generated *in silico* using the CHARMM-GUI membrane-builder.[35] After relaxation of the proteins and the membrane models, we assembled protein-membrane models. For this, we placed each C2 model in three different initial orientations above the lipid membrane (Figure S5) to minimize influence by the starting orientation as reported previously.[36] Performing simulations of C2A and C2B with model membranes mimicking the synaptic vesicle and plasma membrane in the presence and absence of Ca^{2+}, and with three starting orientations, we composed a total of 24 arrangements. Each arrangement was then simulated for 1.5 μs (see STAR Methods for details).

Obtained trajectories confirm that the C2A and C2B domains retain a stable tertiary structure (average Cα root-mean-square deviation <2 Å for all simulations, Figures S6A and S6B). Moreover, inspecting the local flexibility of C2A and C2B, we identified a Ca^{2+}-dependent difference of root-mean-square fluctuation in

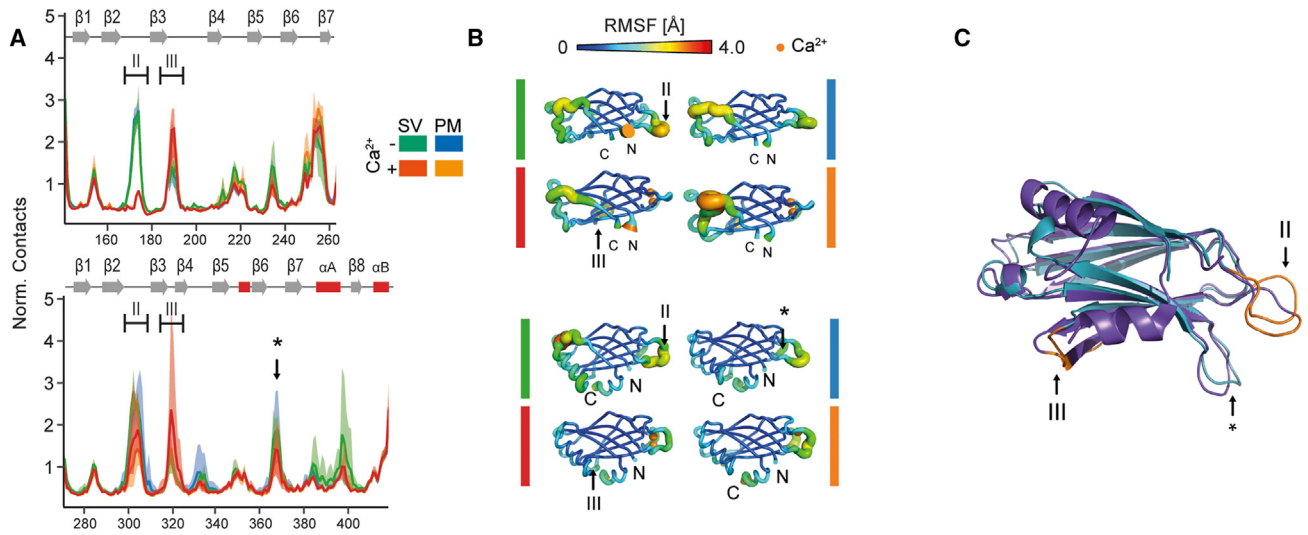

Figure 4. Studying the flexibility of the C2A and C2B domains

(A) Root-mean-square fluctuation (RMSF) of the C2A (top) and C2B (bottom) domains of simulations involving the synaptic vesicle membrane (SV, green, red) and the plasma membrane (PM, blue, orange) in the absence (green, blue) and in the presence (red, orange) of Ca^{2+}. Loop II (residues 169–176 in C2A and residues 300–308 in C2B) and loop III (residues 187–192 in C2A and residues 317–324 in C2B) as well as residues 365–370 in C2B (*) are highlighted. The secondary structure annotation is shown on top of each plot.

(B) RMSF mapped on the structures of the C2 domains of synaptotagmin-1 for selected examples. Higher diameters and warmer colors indicate higher RMSF (see legend).

(C) Structural alignment of the C2A and C2B domains. Regions of flexibility (i.e., loops II, III and * (C2B)) are indicated.

loops II and III of both, C2A and C2B (Figures 4A and 4B). Loop II (residues 169–176 in C2A and residues 300–308 in C2B) represents the calcium-binding region of the C2 domain and a reduced flexibility is in line with binding of Ca^{2+} to this loop. Loop III (residues 187–192 in C2A and residues 317–324 in C2B) showed an increase in root-mean-square fluctuation in the presence of Ca^{2+}; this loop is located on the opposite side of the domain suggesting that Ca^{2+} influences its dynamics indirectly (Figure 4C).

C2A and C2B specifically interact with negatively charged lipids in silico

Having described the structural flexibility of the C2 domains in the absence and presence of Ca^{2+}, we explored their specific interactions with lipids in the simulation. For this, we identified lipid molecules within 2.6 Å (i.e., the distance of a hydrogen bond) of each amino acid residue for each time frame of the simulation and counted the number of residue-lipid contacts throughout the simulation. To eliminate transient, unspecific interactions, we retained only protein-lipid interactions that were observed continuously for at least 10 ns. Contact counts were then normalized by the relative number of lipids in the model membrane excluding stochastic matches and by the total number of lipid contacts in a simulation accounting for varying contact times in different simulations.

Normalized lipid contacts confirm a lipid preference for negatively charged lipids as observed previously *in vitro* (Figure 5A, lhs). Notably, preferential binding was observed to $PI(4,5)P_2$, followed by contacts with PS. Intriguingly, close contacts with PE lipids were also identified, which were not anticipated based on our *in vitro* results. This difference may be attributed to interactions that form in a mixed model membrane, in contrast to the pure lipid compositions as used in native mass spectrometry or lipid overlay experiments, thereby allowing close contacts of the C2 domains with neighboring lipids. Our simulations did not reveal different lipid preferences of the C2A and C2B domains as observed during liposome flotation; however, these differences might originate from binding and unbinding events on a timescale inaccessible to the present simulation. To exploit the atomistic resolution of the simulations, we mapped the residues involved in lipid-contacts on the structural models of C2A and C2B. Binding of $PI(4,5)P_2$ and PS to C2A and C2B predominantly occurred through the calcium-binding loops and the polybasic region for both model membranes in the presence and in the absence of Ca^{2+} (Figure 5A, rhs; Figure 6).

C2A and C2B insert into model membranes

We next examined the insertion of C2A and C2B into the membrane, a phenomenon previously described.[37–39] For this, the closest distance between the C2 domains and the phosphorous atoms of the proximal membrane leaflet was calculated over the last 800 ns of the 1.5 μs simulation time (Figure 5B). Throughout this period, the distances between the C2 domains and the model membrane remained constant, suggesting that the considered time frame represents a (local) energy minimum. Distances >0 Å (see STAR Methods for details on computing the distance) indicate that the protein is located below the phosphate headgroups, i.e., integrates into the membrane, whereas distances <0 Å refer to proteins that do not insert. The histogram of these distances reveals that the insertion depth of C2A shifts from 2.8 to 4.4 Å when Ca^{2+} is included in the simulation, suggesting a tight insertion of C2A into the membrane when Ca^{2+} is present. Importantly, a significant difference in insertion depth of C2A

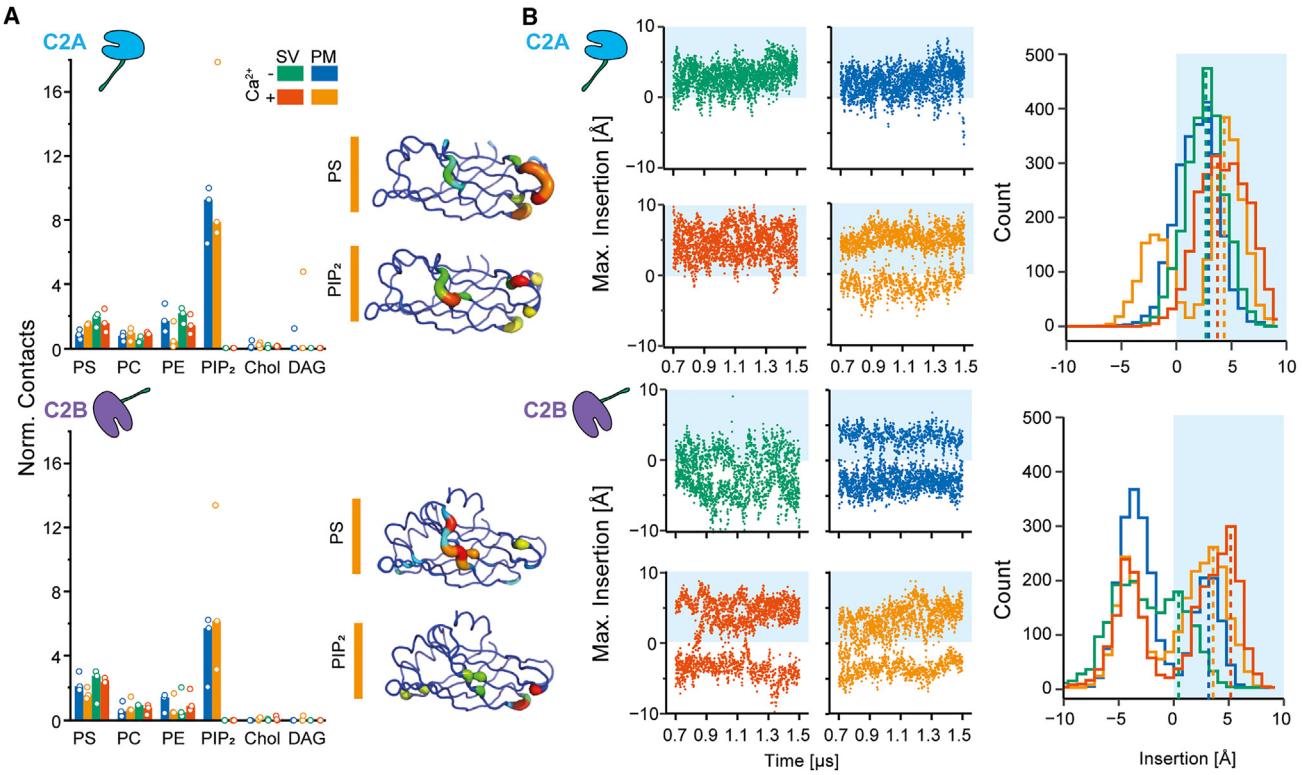

Figure 5. Lipid specificity and membrane insertion of C2A and C2B as identified by molecular dynamics simulations

(A) Normalized lipid contacts of C2A (top) and C2B (bottom) interacting with the synaptic vesicle membrane (SV, green and red) and plasma membrane (PM, blue and orange) in the absence (green and blue) and in the presence (red and orange) of Ca^{2+}. The bar plots (lhs) show the median normalized lipid contacts for C2A (top) and C2B (bottom). Data points indicate summed contacts for each starting condition. Interactions with PS and PIP_2 lipids were mapped on the structural models of C2A (top) and C2B (bottom) domains revealing their contact surfaces. Higher number of lipid contacts is indicated by warmer colors and a larger diameter of the protein backbone representation.

(B) Maximum insertion of the C2 domains during the last 800 ns of the molecular dynamics simulations involving the SV (green and red) and plasma (blue and orange) model membranes in the absence (green and blue) and in the presence (red and orange) of Ca^{2+} (lhs). The corresponding histograms of C2A (top) and C2B (bottom) are shown (rhs). The insertion depth with the highest count is indicated for each condition (dashed lines). The position of the lipid membrane is indicated (blue shaded area).

when interacting with the synaptic vesicle or plasma membrane was not observed. C2B, on the other hand, showed a bimodal distance distribution. Considering only simulation frames in which C2B inserted into the membrane, an increase in insertion depth, similar to C2A, was observed in the presence of Ca^{2+}. Considering the observed counts, a clear trend toward membrane insertion is observed upon Ca^{2+} binding; more precisely, the counts of the bimodal distribution were higher for distances <0 Å in the absence of Ca^{2+} (green and blue simulations in Figure 5B) and higher for distances >0 Å for simulations in the presence of Ca^{2+} (red and orange simulations in Figure 5B). Notably, the insertion depth of C2B into the plasma membrane, when compared with the insertion into the synaptic vesicle membrane, in the absence of Ca^{2+} was comparably high (approximately 3.2 Å) and a stable association with the plasma membrane even in the absence of Ca^{2+} might explain these differences.

Ca^{2+} binding modulates the orientation of C2A and C2B interacting with model membranes

Our analyses showed that the presence of Ca^{2+} leads to a slightly deeper insertion of the C2 domains into both the synaptic vesicle and plasma membranes. We, therefore, further investigated how Ca^{2+} influences the relative orientation of the C2 domains with respect to the membrane. To address this question, we calculated the angle between a vector along the main axis of the C2 domains (Figure 7A; see method details). To exclude the initial annealing phase, we only analyzed the last 800 ns of the simulation time.

This analysis revealed a distinct trend for C2A: in the presence of Ca^{2+}, simulations with either the synaptic vesicle or plasma membrane showed lower contact angles of approximately 45°, corresponding to a more perpendicular orientation on the membrane, while Ca^{2+}-free simulations exhibited average angles of 60°–70°. This finding was consistent across all simulations. Membrane interaction angles observed for C2B, on the other hand, were consistently higher for all membrane systems. A median value of approximately 90° indicates parallel orientation of the C2B main axis to the membrane. Furthermore, in contrast to C2A, distributions of interaction angles were observed for different initial orientations of C2B. For instance, C2B interacting with the plasma membrane in the absence of Ca^{2+} showed an average interaction angle of approximately 95° in simulations

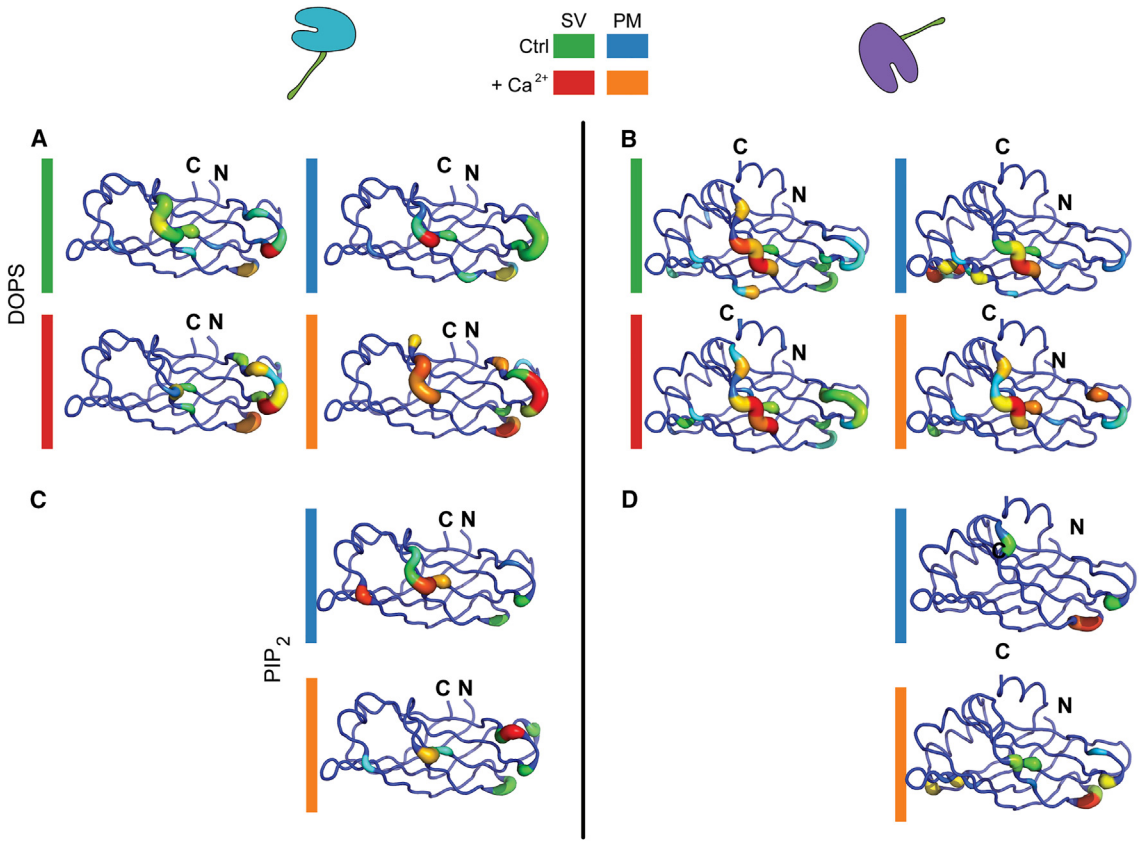

Figure 6. Residues involved in protein-lipid contacts of C2A (cyan, lhs) and C2B (purple, rhs)

The structures of C2A and C2B are shown. Lipid contacts observed in simulations including two model membranes mimicking the synaptic vesicle membrane (SV, green and red) or the plasma membrane (PM, blue and orange) in the absence of Ca^{2+} (Ctrl, green and blue) or in the presence of Ca^{2+} (red and orange). The sum of lipid contacts of three simulations starting with different initial orientations is shown as sausage representation. Warmer colors indicate a higher number of lipid contacts.

(A) Contacts of C2A with DOPS.

(B) Contacts of C2B with DOPS.

(C) Contacts of C2A with PIP_2. Note that PIP_2 is not present in the SV model membrane.

(D) Contacts of C2B with PIP_2. Note that PIP_2 is not present in the SV model membrane.

with 0° or 60° initial orientation, while simulations starting at a 30° angle showed an average final angle of approximately 75° suggesting that C2B interactions with the membrane are more dynamic and at least two membrane orientations, both characterized by higher contact angles than that of C2A, are adopted.

To further investigate the effect of Ca^{2+} binding to the C2 domains on the membrane plane, we analyzed the positions of the membrane phosphorus atoms after binding of C2A or C2B (Figure 7B). For this, we oriented the membrane on the *xy*-plane and centered the C2 domain on the membrane. We then calculated the difference between the *z*-coordinates of the lowest membrane phosphor atom and all other phosphor atoms (see STAR Methods for details). Low distances indicate a planar membrane system, while higher distances suggest local invagination of the membrane. Interestingly, in simulations of C2A, we observed an increase in distance around a central indentation for the proximal leaflet; this effect was pronounced in simulations including Ca^{2+}. Analyzing simulations of C2B revealed a less pronounced effect, even though the indentation for C2B was generally higher in the presence of Ca^{2+}. As a control, we analyzed the phosphorus atoms of the distal leaflet and detected a planar membrane in all simulations (Figure 7B). As expected, the C2 domains appear to affect only one of the two leaflets. These findings agree well with the perpendicular orientation of C2A on the two membrane systems in the presence of Ca^{2+}.

DISCUSSION

In this study, we characterized lipid and membrane binding of the C2A and C2B domains of synaptotagmin-1 in the presence and in the absence of Ca^{2+}. For this, we followed a multidisciplinary approach including lipid overlay assays, native mass spectrometry and liposome flotation assays as well as extensive molecular dynamics simulations. Lipid overlay assays and native mass spectrometry revealed a clear preference for negatively charged phospholipids; of particular interest are PIP_2s, which were previously described to drive Ca^{2+}-dependent interactions of synaptotagmin-1 with the vesicular and the plasma membranes.[28] Employing liposomes as model membranes for synaptic vesicles and the plasma membrane revealed preferences of

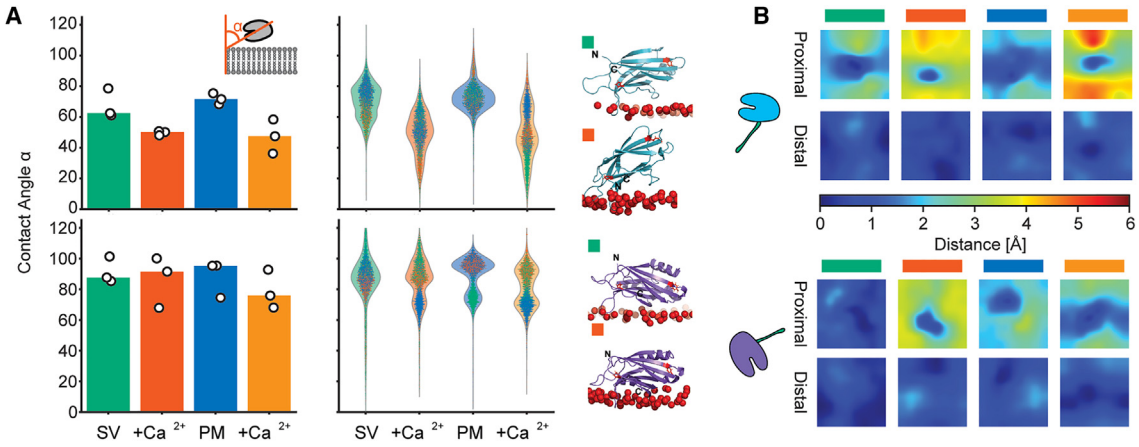

Figure 7. Orientation of C2A and C2B on the SV and plasma model membranes

(A) Median contact angles of C2A (top) and C2B (bottom) with the synaptic vesicle (red and green) and plasma (blue and orange) model membranes (lhs). Angles were averaged over the last 800 ns of the simulation (data points correspond to individual averages for the three initial starting orientations). Violin plots detailing the distributions of contact angles for 0° (violet), 30° (green) and 60° (blue) initial starting orientation (middle panel, data points correspond to individual frames of the simulations). Models representing the orientation of the C2 domains on the SV membrane in the absence (green) and in the presence (red) of Ca^{2+} are shown (rhs).

(B) z-positions of the phosphor atoms of the membrane lipid headgroups in the proximal and distal membrane leaflet of the SV (green and red) and plasma (blue and orange) model membranes when binding C2A (cyan, top) and C2B (purple, bottom) in the absence (green and blue) and in the presence (red and orange) of Ca^{2+}.

C2A and C2B for specific membrane compositions. As described previously, this preference was strongly affected by the presence or absence of Ca^{2+}.[39] Finally, molecular dynamics simulations provided detailed insight into the dynamics of the proteins, the protein-lipid contacts, membrane insertion and local changes in the membrane environment after membrane penetration. While both C2 domains showed very similar lipid contacts and membrane binding behavior during the simulations, differences were mostly observed in the orientation of the domains on the model membranes as well as the effects on the local membrane environment when intruding into the membrane.

Lipid binding to synaptotagmin-1 was assessed in many previous studies, mostly using the cytosolic C2AB construct. To deduce lipid and membrane contacts to the individual C2 domains, we preformed all experiments with isolated C2A and C2B domains. As reported previously, we observed a clear preference for negatively charged phospholipids for both, the C2A and C2B domains, in lipid overlay assays and by native mass spectrometry (Figures 2, 3, and S1). While previous studies mostly targeted PS and PIP_2s, we also observed binding of the C2 domains to additional negatively charged phospholipids such as sulfatides or cardiolipin in lipid overlay assays (Figure 2) or DOPI, DOPI(4)P or DOPI(3,4,5)P3 (Figure S1) in native mass spectrometry measurements. As most of these lipids are physiologically not relevant for synaptotagmin-1, we assume that the C2 domains electrostatically interact with negative charges. Accordingly, using native mass spectrometry, binding of $PI(3,4,5)P_3$ was most pronounced, presumably due to the high negative charges. Importantly, after addition of Ca^{2+}, the preference for negatively charged lipids, in particular for PI(4)P and $PI(4,5)P_2$s, increased in lipid overlay assays; this effect was pronounced for C2B.

Native mass spectrometry, on the other hand, revealed binding of C2A and C2B to all lipids employed here, including zwitterionic DOPC (Figures S1). This interaction was unexpected and might be the result of the experimental approach followed: as the C2A and C2B domains are soluble variants of synaptotagmin-1, we transferred lipids from mixed detergent-lipid micelles onto the proteins during ionization for mass spectrometry experiments.[31] Recently, we characterized protein-lipid interactions that form in solution and are stabilized in the gas-phase and found that protein-lipid interactions in the gas-phase are predominantly stabilized through electrostatic interactions[40]; we therefore assume that interactions with DOPC form through negatively charged residues, e.g., of the Ca^{2+} binding loops, in the presence and in the absence of Ca^{2+} and are, therefore, not relevant for stable protein-lipid contacts. Accordingly, the complexes that formed between the C2 domains and DOPC readily dissociated at low collisional energies in contrast to the complexes that formed with negatively charged phospholipids (Figures S2 and S4A).

Surprisingly, in contrast to a recent study,[41] pre-incubation of the C2 domains with Ca^{2+} or EGTA (to mimic a "real" Ca^{2+}-free state) did not affect the degree of phospholipid binding (Figure S4). Methodological limitations might be the reason for this discrepancy: (1) solvent molecules evaporate during electrospray ionization, and non-covalent interactions in the gas phase are stabilized through electrostatic interactions,[40] i.e., even transient interactions might be captured and stabilized; (2) unspecific interactions between proteins and detergent-lipid micelles might be induced due to shrinking of the electrospray droplet during the ionization process; and (3) instrument parameters had to be adjusted for the analysis in the presence of Ca^{2+} (or EGTA). These analyses required a high collisional voltage at which protein-lipid complexes (at least partially) dissociate; consequently, phospholipid binding is not quantitative under these conditions. The applicability of native mass spectrometry to study Ca^{2+}-dependent phospholipid binding remains to be evaluated in future studies.

Nonetheless, interactions of synaptotagmin-1 with phospholipids are mainly based on electrostatic interaction (e.g., studies by Striegel et al.,[18] Bai et al.,[25] and Brose et al.[42]) and, therefore, native mass spectrometry appears to be well-suited to assess the stability of phospholipid binding. Our findings are in accordance with the commonly accepted hypothesis that synaptotagmin-1 stably binds PS and PIPs/PIP_2s.

Using native mass spectrometry, we further observed binding of up to three lipid molecules per C2 domain (Figures 2 and S1). Assuming membrane binding through the Ca^{2+}-binding loops and the polybasic lysine patches, this binding stoichiometry agrees well with few lipid contacts per domain. In addition to the number of available contact sites on the protein surface, the number of lipid adducts increased with lipid concentration (Figure S1) suggesting a concentration-dependent association.

Having characterized binding of specific lipid molecules, we further assessed binding of the C2 domains to phospholipid bilayers of liposomes mimicking the synaptic vesicle or plasma membrane. While both, C2A and C2B, showed only minimal binding to the liposomes in the absence of Ca^{2+}, clear differences in the preferences for the lipid composition were observed when Ca^{2+} was added. Accordingly, C2A was not selective in the membrane composition, however, C2B showed enhanced binding to the PI(4,5)P_2-containing plasma membrane and only minimal interactions with the synaptic vesicle membrane (Figure 3). This observation agrees well with previous studies suggesting preferred binding of C2B to PI(4,5)P_2 through the polybasic lysine patch.[22,25,39,43–48] Importantly, a different Ca^{2+}-dependent lipid binding behavior was described for the C2A/C2B domains of Rab3A and synaptotagmin-1[48] suggesting that different C2 domains are fine-tuned for their environment (i.e., the lipid composition of the membranes) and for their function (slow versus fast Ca^{2+} sensors). Accordingly, Rab3A is a slow Ca^{2+} sensor (low Ca^{2+} affinity), located at the fusion site, which does not compete with synaptotagmin-1. The different lipid binding properties of the C2 domains are adjusted to their function, i.e., to their target membranes.[48] Our results further support a bridging model, in which C2A interacts with the synaptic vesicles membrane and C2B contacts the plasma membrane.[22,28] While the interface between C2B and the plasma membrane requires specific interactions, C2A is anchored to the vesicle membrane and, therefore, spatially oriented toward the vesicle membrane.

To gain detailed insight into these interactions, molecular dynamics simulations were widely used in the last two decades. However, a direct comparison of the results obtained from these studies is difficult as they differ, for instance, in lipid composition of the model membranes, protein variants (most studies used the C2AB fragment), additional binding partners such as SNARE proteins and, importantly, the simulation time.[37,49,50] In this work, we simulated isolated C2 domains with and without Ca^{2+} to characterize their binding to a complex membrane, designed to mimic the lipid composition employed in membrane fusion experiments.[33] To obtain robust statistics, we simulated each model system in 1.5 μs-long triplicates, initializing the C2 domains at different angles with respect to the membranes (Figure S5). Our resulting description of C2A and C2B interactions with the membrane agrees well with a recent study also including the isolated C2A and C2B domains.[37] Notably, our observation that the C2A domain is not selective in the membrane composition and rather responds to Ca^{2+} binding, while the C2B domain stably associates with the PI(4,5)P_2-containing plasma membrane even in the absence of Ca^{2+} (Figure 5) was previously described experimentally[24,44,45] confirming a good agreement between our simulations and experimental studies.

While the binding behavior of C2A and C2B was comparable in terms of lipid contacts, differences were observed in the orientation of the two domains on the membrane. As suggested previously,[37] C2B adopted a rather flat orientation allowing contacts with lipids through the Ca^{2+}-binding loops and the polybasic patch (Figure 7A). This orientation agrees well with a previous study reporting an orientation parallel to the membrane for C2 domains with type II topology.[51] Notably, a bimodal distribution was observed for the orientation of C2B suggesting a more transient association with the membrane. C2A, on the other hand, adopted a more upright orientation perpendicular to the membrane plane in the presence of Ca^{2+} (Figure 7A). In addition, this upright position induced deeper insertion into the membrane causing local rearrangements of the membrane in the direct neighborhood of the protein (Figure 7B). C2A, therefore, appears to adopt the typical orientation of type I C2 domains in the absence of Ca^{2+}, while the upright orientation in the presence of Ca^{2+} resembles the orientation of type II C2 domains.[51] The change in orientation in the presence of Ca^{2+} suggests a role during membrane fusion by stretching the linker connecting the C2A and C2B domains and, as a consequence, pulling the vesicular and the plasma membranes together. Considering that synaptotagmin-1 contains two C2 domains, while one C2 domain would be sufficient to bridge the two membranes, we propose that this structural change represents an additional regulatory element during membrane fusion.

Finally, our results allow us to propose a mechanistic model showing how membrane interactions of C2A and C2B contribute to membrane fusion (Figure 8). In this model, C2A is binding the synaptic vesicle membrane, while C2B, which is connected through a flexible linker, is moving toward the PI(4,5)P_2-containing plasma membrane. The flexible linker further allows membrane contacts prior to Ca^{2+} binding. Flexibility of C2B allows additional contacts with the SNARE complex as proposed previously.[52,53] Upon Ca^{2+} binding, the C2B domain stably associates with the plasma membrane and C2A adopts an upright orientation at the vesicle membrane. These binding effects cause tension at the connecting flexible linker, thereby pulling the two membranes together (Figure 8). All in all, our model agrees well with previously published models: It includes a bridging mechanism of full-length synaptotagmin-1,[22,28] it allows for contacts with the SNARE complex,[54,55] it involves contacts of C2B with the plasma membrane in the absence of Ca^{2+},[24,44,45] it requires both C2A and C2B domains for membrane fusion[56] and it allows regulation by additional factors such as complexin-1 that interact with the SNARE complex or synaptotagmin-1.[57–59]

STAR★METHODS

Detailed methods are provided in the online version of this paper and include the following:

- KEY RESOURCES TABLE
- RESOURCE AVAILABILITY

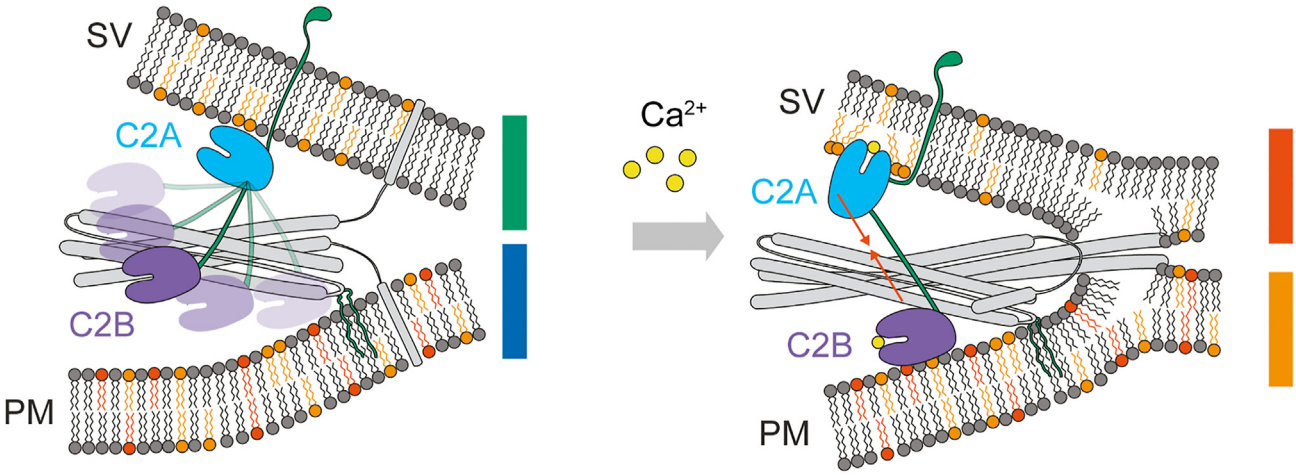

Figure 8. Model summarizing the effects of Ca^{2+} binding on the interactions between C2A and C2B with the membranes

In the absence of Ca^{2+}, C2A interacts with the synaptic vesicle (SV) membrane, while C2B is flexible making contacts with the SNARE complex as well as the plasma membrane (PM). Binding of Ca^{2+} then leads to a perpendicular orientation of C2A and partial penetration into the membrane leaflet, as well as enhanced interactions of C2B with the PM. These structural rearrangements of the C2 domains induce tension on the linker connecting C2A and C2B, thereby, pulling the SV membrane and the PM together.

SUPPLEMENTAL INFORMATION

Supplemental information can be found online at https://doi.org/10.1016/j.str.2024.07.017.

ACKNOWLEDGMENTS

We thank Reinhard Jahn (MPI for Multidisciplinary Sciences, Göttingen, Germany) for providing synaptotagmin-1 plasmids. We acknowledge funding from the Federal Ministry of Education and Research (BMBF, 03Z22HN22 and 03Z22HI2), the European Regional Development Funds (EFRE, ZS/2016/04/78115) and the German Research Foundation (DFG, project number 436494874, RTG 2670 "Beyond Amphiphilicity: Self-Organization of Soft Matter via Multiple Noncovalent Interactions" and project number 391498659, RTG 2467 "Intrinsically Disordered Proteins – Molecular Principles, Cellular Functions, and Diseases"). J. Bender acknowledges funding from the Studienstiftung des Deutschen Volkes. J. Bieber is a Joachim Herz Add-on Fellow. M.T.D. acknowledges funding from the Engineering and Physical Sciences Research Council (fellowship EP/P016499/1).

AUTHOR CONTRIBUTIONS

Conceptualization, J. Bender and C.S.; methodology, J. Bender, L.S.P.R., M.T.D., and C.S.; software, J. Bender and L.S.P.R.; investigation, J. Bender, T.K., M.F., J. Bieber; writing – original draft, J. Bender and C.S.; writing – review & editing, J. Bender, T.K., L.S.P.R., J. Bieber, M.T.D., and C.S.; visualization, J. Bender, T.K., and C.S.; supervision, M.T.D. and C.S.; funding acquisition, M.T.D. and C.S.

DECLARATION OF INTERESTS

The authors declare no competing interest.

Received: February 7, 2024
Revised: July 4, 2024
Accepted: July 28, 2024
Published: August 21, 2024

REFERENCES

1. Jahn, R., and Südhof, T.C. (1994). Synaptic vesicles and exocytosis. Annu. Rev. Neurosci. *17*, 219–246. https://doi.org/10.1146/annurev.ne.17.030194.001251.
2. Sudhof, T.C. (2004). The synaptic vesicle cycle. Annu. Rev. Neurosci. *27*, 509–547. https://doi.org/10.1146/annurev.neuro.26.041002.131412.
3. Sollner, T., Whiteheart, S.W., Brunner, M., Erdjument-Bromage, H., Geromanos, S., Tempst, P., and Rothman, J.E. (1993). SNAP receptors implicated in vesicle targeting and fusion. Nature *362*, 318–324. https://doi.org/10.1038/362318a0.
4. Fasshauer, D., Bruns, D., Shen, B., Jahn, R., and Brünger, A.T. (1997). A structural change occurs upon binding of syntaxin to SNAP-25. J. Biol. Chem. *272*, 4582–4590. https://doi.org/10.1074/jbc.272.7.4582.
5. Fasshauer, D., Otto, H., Eliason, W.K., Jahn, R., and Brünger, A.T. (1997). Structural changes are associated with soluble N-ethylmaleimide-sensitive fusion protein attachment protein receptor complex formation. J. Biol. Chem. *272*, 28036–28041. https://doi.org/10.1074/jbc.272.44.28036.
6. Sutton, R.B., Fasshauer, D., Jahn, R., and Brunger, A.T. (1998). Crystal structure of a SNARE complex involved in synaptic exocytosis at 2.4 A resolution. Nature *395*, 347–353. https://doi.org/10.1038/26412.
7. Gao, Y., Zorman, S., Gundersen, G., Xi, Z., Ma, L., Sirinakis, G., Rothman, J.E., and Zhang, Y. (2012). Single reconstituted neuronal SNARE complexes zipper in three distinct stages. Science *337*, 1340–1343. https://doi.org/10.1126/science.1224492.

8. Min, D., Kim, K., Hyeon, C., Cho, Y.H., Shin, Y.K., and Yoon, T.Y. (2013). Mechanical unzipping and rezipping of a single SNARE complex reveals hysteresis as a force-generating mechanism. Nat. Commun. *4*, 1705. https://doi.org/10.1038/ncomms2692.

9. McMahon, H.T., Missler, M., Li, C., and Südhof, T.C. (1995). Complexins: cytosolic proteins that regulate SNAP receptor function. Cell *83*, 111–119. https://doi.org/10.1016/0092-8674(95)90239-2.

10. Mohrmann, R., Dhara, M., and Bruns, D. (2015). Complexins: small but capable. Cell. Mol. Life Sci. *72*, 4221–4235. https://doi.org/10.1007/s00018-015-1998-8.

11. Xu, J., Mashimo, T., and Südhof, T.C. (2007). Synaptotagmin-1, -2, and -9: Ca(2+) sensors for fast release that specify distinct presynaptic properties in subsets of neurons. Neuron *54*, 567–581. https://doi.org/10.1016/j.neuron.2007.05.004.

12. Perin, M.S., Brose, N., Jahn, R., and Südhof, T.C. (1991). Domain structure of synaptotagmin (p65). J. Biol. Chem. *266*, 623–629.

13. Perin, M.S., Fried, V.A., Mignery, G.A., Jahn, R., and Südhof, T.C. (1990). Phospholipid binding by a synaptic vesicle protein homologous to the regulatory region of protein kinase C. Nature *345*, 260–263. https://doi.org/10.1038/345260a0.

14. Fernandez, I., Araç, D., Ubach, J., Gerber, S.H., Shin, O., Gao, Y., Anderson, R.G., Südhof, T.C., and Rizo, J. (2001). Three-dimensional structure of the synaptotagmin 1 C2B-domain: synaptotagmin 1 as a phospholipid binding machine. Neuron *32*, 1057–1069. https://doi.org/10.1016/s0896-6273(01)00548-7.

15. Shao, X., Fernandez, I., Südhof, T.C., and Rizo, J. (1998). Solution structures of the Ca2+-free and Ca2+-bound C2A domain of synaptotagmin I: does Ca2+ induce a conformational change? Biochemistry *37*, 16106–16115. https://doi.org/10.1021/bi981789h.

16. Sutton, R.B., Davletov, B.A., Berghuis, A.M., Südhof, T.C., and Sprang, S.R. (1995). Structure of the first C2 domain of synaptotagmin I: a novel Ca2+/phospholipid-binding fold. Cell *80*, 929–938. https://doi.org/10.1016/0092-8674(95)90296-1.

17. Ubach, J., Zhang, X., Shao, X., Südhof, T.C., and Rizo, J. (1998). Ca2+ binding to synaptotagmin: how many Ca2+ ions bind to the tip of a C2-domain? EMBO J. *17*, 3921–3930. https://doi.org/10.1093/emboj/17.14.3921.

18. Striegel, A.R., Biela, L.M., Evans, C.S., Wang, Z., Delehoy, J.B., Sutton, R.B., Chapman, E.R., and Reist, N.E. (2012). Calcium binding by synaptotagmin's C2A domain is an essential element of the electrostatic switch that triggers synchronous synaptic transmission. J. Neurosci. *32*, 1253–1260. https://doi.org/10.1523/JNEUROSCI.4652-11.2012.

19. Ali Moussa, H.Y., and Park, Y. (2022). Electrostatic regulation of the cis- and trans-membrane interactions of synaptotagmin-1. Sci. Rep. *12*, 22407. https://doi.org/10.1038/s41598-022-26723-9.

20. Chapman, E.R., and Davis, A.F. (1998). Direct interaction of a Ca2+-binding loop of synaptotagmin with lipid bilayers. J. Biol. Chem. *273*, 13995–14001. https://doi.org/10.1074/jbc.273.22.13995.

21. Zhang, X., Rizo, J., and Südhof, T.C. (1998). Mechanism of phospholipid binding by the C2A-domain of synaptotagmin I. Biochemistry *37*, 12395–12403. https://doi.org/10.1021/bi9807512.

22. Arac, D., Chen, X., Khant, H.A., Ubach, J., Ludtke, S.J., Kikkawa, M., Johnson, A.E., Chiu, W., Sudhof, T.C., and Rizo, J. (2006). Close membrane-membrane proximity induced by Ca(2+)-dependent multivalent binding of synaptotagmin-1 to phospholipids. Nat. Struct. Mol. Biol. *13*, 209–217. https://doi.org/10.1038/nsmb1056.

23. Radhakrishnan, A., Stein, A., Jahn, R., and Fasshauer, D. (2009). The Ca2+ affinity of synaptotagmin 1 is markedly increased by a specific interaction of its C2B domain with phosphatidylinositol 4,5-bisphosphate. J. Biol. Chem. *284*, 25749–25760. https://doi.org/10.1074/jbc.M109.042499.

24. van den Bogaart, G., Meyenberg, K., Diederichsen, U., and Jahn, R. (2012). Phosphatidylinositol 4,5-bisphosphate increases Ca2+ affinity of synaptotagmin-1 by 40-fold. J. Biol. Chem. *287*, 16447–16453. https://doi.org/10.1074/jbc.M112.343418.

25. Bai, J., Tucker, W.C., and Chapman, E.R. (2004). PIP2 increases the speed of response of synaptotagmin and steers its membrane-penetration activity toward the plasma membrane. Nat. Struct. Mol. Biol. *11*, 36–44. https://doi.org/10.1038/nsmb709.

26. Bhalla, A., Tucker, W.C., and Chapman, E.R. (2005). Synaptotagmin isoforms couple distinct ranges of Ca2+, Ba2+, and Sr2+ concentration to SNARE-mediated membrane fusion. Mol. Biol. Cell *16*, 4755–4764. https://doi.org/10.1091/mbc.e05-04-0277.

27. Bradberry, M.M., Bao, H., Lou, X., and Chapman, E.R. (2019). Phosphatidylinositol 4,5-bisphosphate drives Ca(2+)-independent membrane penetration by the tandem C2 domain proteins synaptotagmin-1 and Doc2beta. J. Biol. Chem. *294*, 10942–10953. https://doi.org/10.1074/jbc.RA119.007929.

28. Nyenhuis, S.B., Thapa, A., and Cafiso, D.S. (2019). Phosphatidylinositol 4,5 Bisphosphate Controls the cis and trans Interactions of Synaptotagmin 1. Biophys. J. *117*, 247–257. https://doi.org/10.1016/j.bpj.2019.06.016.

29. Park, Y., and Ryu, J.K. (2018). Models of synaptotagmin-1 to trigger Ca(2+)-dependent vesicle fusion. FEBS Lett. *592*, 3480–3492. https://doi.org/10.1002/1873-3468.13193.

30. Llinas, R., Sugimori, M., and Silver, R.B. (1992). Microdomains of high calcium concentration in a presynaptic terminal. Science *256*, 677–679. https://doi.org/10.1126/science.1350109.

31. Landreh, M., Costeira-Paulo, J., Gault, J., Marklund, E.G., and Robinson, C.V. (2017). Effects of Detergent Micelles on Lipid Binding to Proteins in Electrospray Ionization Mass Spectrometry. Anal. Chem. *89*, 7425–7430. https://doi.org/10.1021/acs.analchem.7b00922.

32. Steinberg, M.Z., Elber, R., McLafferty, F.W., Gerber, R.B., and Breuker, K. (2008). Early structural evolution of native cytochrome c after solvent removal. Chembiochem *9*, 2417–2423. https://doi.org/10.1002/cbic.200800167.

33. Liu, X., Seven, A.B., Xu, J., Esser, V., Su, L., Ma, C., and Rizo, J. (2017). Simultaneous lipid and content mixing assays for *in vitro* reconstitution studies of synaptic vesicle fusion. Nat. Protoc. *12*, 2014–2028. https://doi.org/10.1038/nprot.2017.068.

34. Lyubimov, A.Y., Uervirojnangkoorn, M., Zeldin, O.B., Zhou, Q., Zhao, M., Brewster, A.S., Michels-Clark, T., Holton, J.M., Sauter, N.K., Weis, W.I., and Brunger, A.T. (2016). Advances in X-ray free electron laser (XFEL) diffraction data processing applied to the crystal structure of the synaptotagmin-1/SNARE complex. Elife *5*, e18740. https://doi.org/10.7554/eLife.18740.

35. Wu, E.L., Cheng, X., Jo, S., Rui, H., Song, K.C., Dávila-Contreras, E.M., Qi, Y., Lee, J., Monje-Galvan, V., Venable, R.M., et al. (2014). CHARMM-GUI Membrane Builder toward realistic biological membrane simulations. J. Comput. Chem. *35*, 1997–2004. https://doi.org/10.1002/jcc.23702.

36. Chon, N.L., Osterberg, J.R., Henderson, J., Khan, H.M., Reuter, N., Knight, J.D., and Lin, H. (2015). Membrane Docking of the Synaptotagmin 7 C2A Domain: Computation Reveals Interplay between Electrostatic and Hydrophobic Contributions. Biochemistry *54*, 5696–5711. https://doi.org/10.1021/acs.biochem.5b00422.

37. Bykhovskaia, M. (2021). SNARE complex alters the interactions of the Ca(2+) sensor synaptotagmin 1 with lipid bilayers. Biophys. J. *120*, 642–661. https://doi.org/10.1016/j.bpj.2020.12.025.

38. Herrick, D.Z., Sterbling, S., Rasch, K.A., Hinderliter, A., and Cafiso, D.S. (2006). Position of synaptotagmin I at the membrane interface: cooperative interactions of tandem C2 domains. Biochemistry *45*, 9668–9674. https://doi.org/10.1021/bi060874j.

39. Perez-Lara, A., Thapa, A., Nyenhuis, S.B., Nyenhuis, D.A., Halder, P., Tietzel, M., Tittmann, K., Cafiso, D.S., and Jahn, R. (2016). PtdInsP2 and PtdSer cooperate to trap synaptotagmin-1 to the plasma membrane in the presence of calcium. Elife *5*, e15886. https://doi.org/10.7554/eLife.15886.

40. Kundlacz, T., and Schmidt, C. (2023). Deciphering Solution and Gas-Phase Interactions between Peptides and Lipids by Native Mass Spectrometry. Anal. Chem. *95*, 17292–17299. https://doi.org/10.1021/acs.analchem.3c03428.

41. Lawrence, S.A.S., Kirschbaum, C., Bennett, J.L., Lutomski, C.A., El-Baba, T.J., and Robinson, C.V. (2024). Phospholipids Differentially Regulate Ca(2+) Binding to Synaptotagmin-1. ACS Chem. Biol. *19*, 953–961. https://doi.org/10.1021/acschembio.3c00772.

42. Brose, N., Petrenko, A.G., Südhof, T.C., and Jahn, R. (1992). Synaptotagmin: a calcium sensor on the synaptic vesicle surface. Science *256*, 1021–1025. https://doi.org/10.1126/science.1589771.

43. Honigmann, A., van den Bogaart, G., Iraheta, E., Risselada, H.J., Milovanovic, D., Mueller, V., Müllar, S., Diederichsen, U., Fasshauer, D., Grubmüller, H., et al. (2013). Phosphatidylinositol 4,5-bisphosphate clusters act as molecular beacons for vesicle recruitment. Nat. Struct. Mol. Biol. *20*, 679–686. https://doi.org/10.1038/nsmb.2570.

44. Li, L., Shin, O.H., Rhee, J.S., Araç, D., Rah, J.C., Rizo, J., Südhof, T., and Rosenmund, C. (2006). Phosphatidylinositol phosphates as co-activators of Ca2+ binding to C2 domains of synaptotagmin 1. J. Biol. Chem. *281*, 15845–15852. https://doi.org/10.1074/jbc.M600888200.

45. Park, Y., Seo, J.B., Fraind, A., Pérez-Lara, A., Yavuz, H., Han, K., Jung, S.R., Kattan, I., Walla, P.J., Choi, M., et al. (2015). Synaptotagmin-1 binds to PIP(2)-containing membrane but not to SNAREs at physiological ionic strength. Nat. Struct. Mol. Biol. *22*, 815–823. https://doi.org/10.1038/nsmb.3097.

46. van den Bogaart, G., Meyenberg, K., Risselada, H.J., Amin, H., Willig, K.I., Hubrich, B.E., Dier, M., Hell, S.W., Grubmüller, H., Diederichsen, U., and Jahn, R. (2011). Membrane protein sequestering by ionic protein-lipid interactions. Nature *479*, 552–555. https://doi.org/10.1038/nature10545.

47. Wang, Z., Liu, H., Gu, Y., and Chapman, E.R. (2011). Reconstituted synaptotagmin I mediates vesicle docking, priming, and fusion. J. Cell Biol. *195*, 1159–1170. https://doi.org/10.1083/jcb.201104079.

48. Guillen, J., Ferrer-Orta, C., Buxaderas, M., Perez-Sanchez, D., Guerrero-Valero, M., Luengo-Gil, G., Pous, J., Guerra, P., Gomez-Fernandez, J.C., Verdaguer, N., et al. (2013). Structural insights into the Ca2+ and PI(4,5)P2 binding modes of the C2 domains of rabphilin 3A and synaptotagmin 1. Proc. Natl. Acad. Sci. USA *110*, 20503–20508. https://doi.org/10.1073/pnas.1316179110.

49. Prasad, R., and Zhou, H.X. (2020). Membrane Association and Functional Mechanism of Synaptotagmin-1 in Triggering Vesicle Fusion. Biophys. J. *119*, 1255–1265. https://doi.org/10.1016/j.bpj.2020.08.008.

50. Rizo, J., Sari, L., Qi, Y., Im, W., and Lin, M.M. (2022). All-atom molecular dynamics simulations of Synaptotagmin-SNARE-complexin complexes bridging a vesicle and a flat lipid bilayer. Elife *11*, e76356. https://doi.org/10.7554/eLife.76356.

51. Larsen, A.H., and Sansom, M.S.P. (2021). Binding of Ca(2+)-independent C2 domains to lipid membranes: A multi-scale molecular dynamics study. Structure *29*, 1200–1213.e2. https://doi.org/10.1016/j.str.2021.05.011.

52. Vrljic, M., Strop, P., Ernst, J.A., Sutton, R.B., Chu, S., and Brunger, A.T. (2010). Molecular mechanism of the synaptotagmin-SNARE interaction in Ca2+-triggered vesicle fusion. Nat. Struct. Mol. Biol. *17*, 325–331. https://doi.org/10.1038/nsmb.1764.

53. Zhou, Q., Lai, Y., Bacaj, T., Zhao, M., Lyubimov, A.Y., Uervirojnangkoorn, M., Zeldin, O.B., Brewster, A.S., Sauter, N.K., Cohen, A.E., et al. (2015). Architecture of the synaptotagmin-SNARE machinery for neuronal exocytosis. Nature *525*, 62–67. https://doi.org/10.1038/nature14975.

54. Chicka, M.C., Hui, E., Liu, H., and Chapman, E.R. (2008). Synaptotagmin arrests the SNARE complex before triggering fast, efficient membrane fusion in response to Ca2+. Nat. Struct. Mol. Biol. *15*, 827–835. https://doi.org/10.1038/nsmb.1463.

55. Wang, S., Li, Y., and Ma, C. (2016). Synaptotagmin-1 C2B domain interacts simultaneously with SNAREs and membranes to promote membrane fusion. Elife *5*, e14211. https://doi.org/10.7554/eLife.14211.

56. Wu, Z., Ma, L., Courtney, N.A., Zhu, J., Landajuela, A., Zhang, Y., Chapman, E.R., and Karatekin, E. (2022). Polybasic Patches in Both C2 Domains of Synaptotagmin-1 Are Required for Evoked Neurotransmitter Release. J. Neurosci. *42*, 5816–5829. https://doi.org/10.1523/JNEUROSCI.1385-21.2022.

57. Jaczynska, K., Esquivies, L., Pfuetzner, R.A., Alten, B., Brewer, K.D., Zhou, Q., Kavalali, E.T., Brunger, A.T., and Rizo, J. (2023). Analysis of tripartite Synaptotagmin-1-SNARE-complexin-1 complexes in solution. FEBS Open Bio *13*, 26–50. https://doi.org/10.1002/2211-5463.13503.

58. Zdanowicz, R., Kreutzberger, A., Liang, B., Kiessling, V., Tamm, L.K., and Cafiso, D.S. (2017). Complexin Binding to Membranes and Acceptor t-SNAREs Explains Its Clamping Effect on Fusion. Biophys. J. *113*, 1235–1250. https://doi.org/10.1016/j.bpj.2017.04.002.

59. Zhou, Q., Zhou, P., Wang, A.L., Wu, D., Zhao, M., Südhof, T.C., and Brunger, A.T. (2017). The primed SNARE-complexin-synaptotagmin complex for neuronal exocytosis. Nature *548*, 420–425. https://doi.org/10.1038/nature23484.

60. Stein, A., Radhakrishnan, A., Riedel, D., Fasshauer, D., and Jahn, R. (2007). Synaptotagmin activates membrane fusion through a Ca2+-dependent trans interaction with phospholipids. Nat. Struct. Mol. Biol. *14*, 904–911. https://doi.org/10.1038/nsmb1305.

61. Berendsen, H.J.C., Vanderspoel, D., and Vandrunen, R. (1995). Gromacs - a Message-Passing Parallel Molecular-Dynamics Implementation. Comput. Phys. Commun. *91*, 43–56. https://doi.org/10.1016/0010-4655(95)00042-E.

62. Jo, S., Kim, T., Iyer, V.G., and Im, W. (2008). CHARMM-GUI: a web-based graphical user interface for CHARMM. J. Comput. Chem. *29*, 1859–1865. https://doi.org/10.1002/jcc.20945.

63. Lee, J., Cheng, X., Swails, J.M., Yeom, M.S., Eastman, P.K., Lemkul, J.A., Wei, S., Buckner, J., Jeong, J.C., Qi, Y., et al. (2016). CHARMM-GUI Input Generator for NAMD, GROMACS, AMBER, OpenMM, and CHARMM/OpenMM Simulations Using the CHARMM36 Additive Force Field. J. Chem. Theor. Comput. *12*, 405–413. https://doi.org/10.1021/acs.jctc.5b00935.

64. Humphrey, W., Dalke, A., and Schulten, K. (1996). VMD: visual molecular dynamics. J. Mol. Graph. *14*, 33. https://doi.org/10.1016/0263-7855(96)00018-5.

65. Nagy, G., Igaev, M., Jones, N.C., Hoffmann, S.V., and Grubmüller, H. (2019). SESCA: Predicting Circular Dichroism Spectra from Protein Molecular Structures. J. Chem. Theor. Comput. *15*, 5087–5102. https://doi.org/10.1021/acs.jctc.9b00203.

66. Marty, M.T., Baldwin, A.J., Marklund, E.G., Hochberg, G.K.A., Benesch, J.L.P., and Robinson, C.V. (2015). Bayesian deconvolution of mass and ion mobility spectra: from binary interactions to polydisperse ensembles. Anal. Chem. *87*, 4370–4376. https://doi.org/10.1021/acs.analchem.5b00140.

67. Michaud-Agrawal, N., Denning, E.J., Woolf, T.B., and Beckstein, O. (2011). MDAnalysis: a toolkit for the analysis of molecular dynamics simulations. J. Comput. Chem. *32*, 2319–2327. https://doi.org/10.1002/jcc.21787.

68. Herrick, D.Z., Kuo, W., Huang, H., Schwieters, C.D., Ellena, J.F., and Cafiso, D.S. (2009). Solution and membrane-bound conformations of the tandem C2A and C2B domains of synaptotagmin 1: Evidence for bilayer bridging. J. Mol. Biol. *390*, 913–923. https://doi.org/10.1016/j.jmb.2009.06.007.

69. Kelly, S.M., Jess, T.J., and Price, N.C. (2005). How to study proteins by circular dichroism. Biochim. Biophys. Acta *1751*, 119–139. https://doi.org/10.1016/j.bbapap.2005.06.005.

70. Sobott, F., Hernández, H., McCammon, M.G., Tito, M.A., and Robinson, C.V. (2002). A tandem mass spectrometer for improved transmission and analysis of large macromolecular assemblies. Anal. Chem. *74*, 1402–1407. https://doi.org/10.1021/ac0110552.

71. Hernandez, H., and Robinson, C.V. (2007). Determining the stoichiometry and interactions of macromolecular assemblies from mass spectrometry. Nat. Protoc. *2*, 715–726. https://doi.org/10.1038/nprot.2007.73.

72. Huang, J., Rauscher, S., Nawrocki, G., Ran, T., Feig, M., de Groot, B.L., Grubmüller, H., and MacKerell, A.D., Jr. (2017). CHARMM36m: an improved force field for folded and intrinsically disordered proteins. Nat. Methods *14*, 71–73. https://doi.org/10.1038/nmeth.4067.

73. Virtanen, P., Gommers, R., Oliphant, T.E., Haberland, M., Reddy, T., Cournapeau, D., Burovski, E., Peterson, P., Weckesser, W., Bright, J., et al. (2020). SciPy 1.0: fundamental algorithms for scientific computing in Python. Nat. Methods *17*, 261–272. https://doi.org/10.1038/s41592-019-0686-2.

STAR★METHODS

KEY RESOURCES TABLE

REAGENT or RESOURCE	SOURCE	IDENTIFIER
Antibodies		
anti-Synaptotagmin-1 cytoplasmic tail antibody, monoclonal IgG2a mouse antibody	SynapticSystems, Göttingen, Germany	cat. no. 105011; RRID: AB_2619760
anti-6xHis tag antibody, monoclonal IgG2b mouse antibody	Abcam, Cambridge, UK	cat. no. ab18184; RRID: AB_444306
peroxidase-coupled anti-mouse IgG secondary antibody, polyclonal IgG2 rabbit antibody	Sigma Aldrich. St. Louis, U.S.A.	cat. no. A9044; RRID: AB_258431
Bacterial and virus strains		
E. coli BL21 (DE3)	New England Biolabs	cat. no. C2527I
Chemicals, peptides, and recombinant proteins		
DOPS	Avanti Polar Lipids	cat. no. 840035
DOPC	Avanti Polar Lipids	cat. no. 850375
DOPE	Avanti Polar Lipids	cat. no. 850725
DOPI	Avanti Polar Lipids	cat. no. 850149
DOPI(4)P	Avanti Polar Lipids	cat. no. 850151
DOPI(4,5)P_2	Avanti Polar Lipids	cat. no. 850155
DOPI(3,4,5)P_3	Avanti Polar Lipids	cat. no. 850156
Cholesterol	Avanti Polar Lipids	cat. no. 700100
DAG	Avanti Polar Lipids	cat. no. 800815
Critical commercial assays		
Membrane lipid strips	Echelon Biosciences	cat. no. P-6002
Deposited data		
MD trajectory files	This paper	https://doi.org/10.5281/zenodo.10478556
Python scripts for MD analysis	This paper	https://github.com/cschmidtlab/syt1_membrane_md
Recombinant DNA		
pET28a Syt-1 C2A Rattus Norvegicus Syt-1 (97-263)	Stein et al.[60]	N/A
pET28a Syt-1 C2B Rattus Norvegicus Syt-1 (271-421)	Stein et al.[60]	N/A
Software and algorithms		
SpectraManager	JASCO	N/A
MassLynx v4.1	Waters	N/A
Kalliope	Anton Paar	N/A
Gromacs 2020.4	Berendsen et al.[61]	www.gromacs.org
CHARRM-Gui	Jo et al.[62]; Lee et al.[63]	www.charmm-gui.org
vmd	Humphrey et al.[64]	https://www.ks.uiuc.edu/Research/vmd/
md-python v3.0.6	www.python.org	N/A
SESCA	Nagy et al.[65]	https://www.mpinat.mpg.de/sesca
Unidec	Marty et al.[66]	https://github.com/michaelmarty/UniDec/releases
MDanalysis v2.5.0	Michaud-Agrawal et al.[67]	www.mdanalysis.org
open source PyMol	www.pymol.org	https://github.com/schrodinger/pymol-open-source

RESOURCE AVAILABILITY

Lead contact

Further information and requests for resources and reagents should be directed to and will be fulfilled by the lead contact, Carla Schmidt (carla.schmidt@uni-mainz.de).

Materials availability

This study did not generate new unique reagents.

Data and code availability

- All MD trajectories have been deposited at Zenodo and are publicly available as of the date of publication (see key resources table for details).
- The Python scripts are available at GitHub and are publicly available as of the date of publication (see key resources table for details).
- Any additional information required to reanalyze the data reported in this paper is available from the lead contact upon request.

EXPERIMENTAL MODEL AND STUDY PARTICIPANT DETAILS

Escherichia coli BL21 (DE3) cells were obtained from New England Biolabs (cat: # C2527I). Cells were first grown in LB media at 37°C and, for expression of the proteins, grown in TB medium (12 g/L tryptone, 24 g/L yeast extract, 0.4%(v/v) glycerol, 2.31 g/L KH2PO4, 12.54 g/L K2HPO4).

METHOD DETAILS

Purification of Synaptotagmin-1 C2A and C2B domains

His-tagged C2A and C2B domains of Synaptotagmin-1 from *Rattus norvegicus* were expressed in *E. coli* and purified as previously described.[39,68] Briefly, C2A and C2B expressing *E. coli* BL21 pET28a cells were disrupted by high pressure and the proteins were purified through the His-tags using a HisTrap HP 5 mL column (GE Healthcare) equilibrated in 20 mM HEPES, 300 mM NaCl, 0.1 mM TCEP, pH 7.4. Bound C2A or C2B domains were eluted with increasing amounts of imidazole. The His-tag was cleaved by thrombin and imidazole was removed during dialysis over night against 20 mM HEPES, 300 mM NaCl, 0.1 mM TCEP, pH 7.4. Cleavage of the His-tag was verified by gel electrophoresis. The His-tag and uncleaved protein were then removed by reversed affinity purification collecting the flow-through. Bound Ni^{2+} ions were removed during dialysis against 20 mM HEPES, 300 mM NaCl, 1 mM EDTA, 0.1 mM TCEP, pH 7.4.

Contaminants such as nucleic acids were removed by ion exchange chromatography using a HiTrap Q HP column (GE Healthcare) equilibrated in 20 mM HEPES, 0.1 mM TCEP, pH 7.4. The protein was eluted with increasing concentrations of NaCl. Protein purity was verified by gel electrophoresis. Peak fractions were concentrated to >1.5 mg/mL using 10 kDa MWCO filtration devices (Amicon).

Gel electrophoresis

Gel electrophoresis was performed using the NuPAGE system according to manufacturer's protocols (Thermo Fisher). The proteins were stained with colloidal Coomassie using InstantBlue Protein stain (Expedeon).

Far-UV CD spectroscopy

The protein concentration was adjusted to < 1 mg/ml with 20 mM HEPES, 300 mM NaCl, 0.1 mM TCEP, pH 7.4. 50 μl of protein solution were transferred into a 0.1 mm quartz cuvette. The ellipticity was recorded at 8°C from 250 to198 nm in continuous scanning mode with a sensitivity of 100 mdeg and a data pitch of 1 nm using a J-810 spectropolarimeter (JASCO). 64 scans, recorded at a scanning speed of 50 nm/min, were accumulated for each spectrum. A reference spectrum of the buffer was subtracted from the recorded spectrum and single binominal smoothing was applied using the SpectraManager software (JASCO). CD spectra were recorded at photomultiplier amplification voltages < 600 V to remove high noise regions. Raw ellipticity was converted to mean residue weighted ellipticity as described.[69] Theoretical reference spectra were calculated from PDB files of the respective domains obtained from full-length Synaptotagmin-1 (PDB: 5KJ7)[34] using SESCA[65] applying standard settings.

Lipid overlay assay

Membrane lipid strips (Echelon Biosciences) were first blocked with 2 mg/ml bovine serum albumin in 50 mM Tris-HCL, 150 mM NaCl, 0.1 % (v/v) Tween 20 for 1 h. Approx. 100 nM C2A or C2B-His in the same buffer containing 1 mM EGTA or 500 μM $CaCl_2$ were then added to the strips followed by incubation at 4°C overnight. The lipid strips were washed at least three times with 50 mM Tris-HCL, 150 mM NaCl, 0.1 % (v/v) Tween 20 and subsequently incubated with 1:1.000 anti-Synaptotagmin-1 cytoplasmic tail (C2A; monoclonal IgG2a mouse antibody, epitope: AA150-240 rat Synaptotagtmin-1, cat. no. 105011, SynapticSystems, Göttingen, Germany) or 1:1.000

anti-6xHis (C2B; monoclonal IgG2b mouse antibody, cat. no. ab18184, abcam, Cambridge, UK) antibodies overnight at 4°C. Again, the lipid strips were washed at least three times using 50 mM Tris-HCL, 150 mM NaCl, 0.1 % (v/v) Tween 20. Subsequently, 1:7.000 peroxidase-coupled anti-mouse IgG secondary antibody (polyclonal IgG2 rabbit antibody, cat. no. A9044, Sigma-Aldrich, St. Louis, U.S.A.) was added and incubated at 4°C overnight. Lipid strips were washed several times with 50 mM Tris-HCL, 150 mM NaCl, 0.1 % (v/v) Tween 20 before a final washing step with water was performed. Binding of the secondary antibody was visualised by chemiluminescence using the ECL detection kit according to manufacturer's protocols (Thermo Fisher Scientific).

Native mass spectrometry

Preparation of detergent-lipid micelles

Mixed detergent-lipid micelles were prepared by sonicating a 1 mM or 300 μM lipid stock solution in 200 mM ammonium acetate solution containing 2 × cmc C8E4 for 30 min.

Lipid binding to C2A and C2B

The purification buffer of the C2A or C2B domain was exchanged against 200 mM ammonium acetate solution containing 2 × cmc C8E4 using 10 kDa MWCO Amicon Ultra Centrifugal Filter according to manufacturer's protocols (Merck Millipore). 10 μM C2A or C2B were mixed with varying lipid-detergent concentrations. Protein-lipid complexes were subsequently analysed on a Synapt G1 HDMS quadrupole time-of-flight mass spectrometer modified for transmission of high-mass complexes.[70] For this, the samples were loaded into in-house prepared gold-coated emitters[71] and the source pressure was adjusted to 5 mbar. Typical instrument parameters were: capillary voltage, 1.7 kV; sampling cone voltage, 30 V; extraction cone voltage, 0.3 V; collision voltage, 10 V; nanoflow pressure, 0.0-0.5 bar; trap cell pressure, 3.5-4 bar. Mass spectra were smoothed twice with MassLynx v4.1 (Waters) applying the Savitzky–Golay filter and a smooth window of 25. Mass spectra were analysed with UniDec software[66] applying the following parameters: m/z range, 1800 to 5000; Charge range 2+ to 10+; Mass range 17000 to 22000 Da.

Lipid binding to C2A and C2B in the absence/presence of Ca^{2+}

60 μM C2A or C2B were pre-incubated for 30 mins with 1mM EGTA in 200 mM ammonium acetate, pH 7.4 (Ca^{2+}-free conditions) or 500 mM $CaCl_2$ in 200 mM AmAc, pH 7.4 (presence of Ca^{2+}) followed by dilution to 10 μM during buffer exchange against 200 mM ammonium acetate using 10 kDa MWCO Amicon Ultra Centrifugal Filter according to manufacturer's protocols (Merck Millipore). DOPC, DOPS or DOPI(4,5)P_2 were dissolved in 0.5 % (w/v) C8E4 and added at a protein:lipid ratio of 1:2.5. The samples were loaded into in-house prepared gold-coated emitters[71] and protein-lipid complexes were analysed on a Waters Micromass QToF Ultima mass spectrometer modified for native mass spectrometry[70] employing the following instrument parameters: capillary voltage, 1.5 kV; cone voltage, 80 V; collision voltage, 60 V. Mass spectra were smoothed twice applying the Savitzky-Golay filter and a smooth window of 10. Mass spectra were analysed with MassLynx v4.1 (Waters).

Liposome preparation and protein binding

Liposomes resembling the synaptic vesicle membrane contained DOPC:DOPS:DOPE:Cholesterol at a molar ratio of 38:12:20:20 and liposomes resembling the presynaptic plasma membrane contained DOPC:DOPS:DOPE:PI(4,5)P_2:DAG:Cholesterol at a molar ratio of 38:12:20:2:2:20.[33] For liposome preparation, lipid mixtures were dissolved in methanol/chloroform (2:1, vol/vol) to a final concentration of 4 mM lipids. Subsequently, the solvent was evaporated and the dry lipid film was hydrated at room temperature for 1 h to a final concentration of 2 mM lipids in 20 mM HEPES, 150 mM KCl, 0.1 mM TCEP, pH 7.4 containing 1 mM EGTA or 100 μM $CaCl_2$. Liposomes of a homogeneous size distribution were obtained by extrusion through a 100 nm polycarbonate membrane for 21 strokes. To study binding of C2A and C2B to the liposome membrane, proteins and liposomes were mixed at 1:250 and 1:1000 protein:lipid ratios followed by incubation for 1h.

Dynamic light scattering

Size distributions of the liposomes were evaluated by dynamic light scattering using a Litesizer 500 (Anton Paar) particle size analyzer equipped with a 633-nm helium-neon laser at a detection angle of 90°. For this, samples were heated for 2 min at 25°C and subsequently analysed 5 times for 15 seconds at 22°C in aqueous buffer. Autocorrelation functions were fitted by applying the Kalliope software (Anton Paar).

Liposome flotation analysis

Binding of C2A or C2B to the liposome membrane was investigated by flotation of the liposomes on a sucrose gradient. For this, liposomes pre-incubated with C2A or C2B, respectively, were mixed with sucrose in 20 mM HEPES, 150 mM KCl, 0.1 mM TCEP, pH 7.4 containing 1 mM EGTA or 100 μM $CaCl_2$ at a final concentration of 1 M. 3/4 volumes of 0.75 M sucrose in the same buffer and 0.175 volumes of buffer were layered on top followed by centrifugation at 268,000 × g for >2 h. Liposomes and bound C2A or C2B migrate to lower sucrose concentrations, while free protein remains in the bottom fraction of the gradient. Top, middle and bottom fractions were collected and top and bottom fractions were inspected by gel electrophoresis.

Molecular dynamics simulations

Equilibration of individual C2 domains

Starting coordinates of C2A (residues 141-263) and C2B (residues 272-418) in the presence of Ca^{2+} were obtained from PDB: 5KJ7 chain K.[34] For simulations in the absence of Ca^{2+}, Ca^{2+} atoms were removed from the structures. Structural models were placed in a

box of TIP3P water with 150 mM K^+ and Cl^- ions at a ratio neutralising the net charge. Structures were relaxed by energy minimization at a maximum force < 1,000 kJ mol^{-1} nm^{-1} followed by 500 ps equilibration in the NVT ensemble (i.e. at a constant number of particles (N), volume (V) and temperature (T)) at 300 K, 500 ps in the NPT ensemble (i.e. at a constant number of particles (N), pressure (P) and temperature (T)) at 1 bar pressure restraining all heavy atoms and 10 ns in the NPT ensemble removing all restraints. Simulations were performed using GROMACS version 2020.4[61] and the CHARMM36m force field.[72] The particle mesh Ewald method was used employing a 10 Å cut-off for calculating long-range electrostatics in the absence of lipids and a 12 Å cut-off in the presence of lipids. The V-rescale modified Berendsen thermostat with separate coupling groups for protein and solvent, and the Berendsen barostat were employed. H-Bonds were constrained using the LINCS algorithm enabling a time step of 2 fs. The final frame of the simulation was used for setting up the protein/membrane simulations.

Equilibration of isolated synaptic vesicle and plasma membrane bilayers

Lipid bilayer structures were obtained from CHARMM-GUI[62,63] specifying a box size of 76 Å edge length, 22.5 Å water layer thickness and a concentration of 150 mM K^+ and Cl^- ions. Membranes were composed of POPC:DOPS:POPE:Cholesterol:PIP_2:DAG (CHARMM-GUI identifiers for PIP_2 and DAG were POPI25 and POGL, respectively) at a ratio of 38:18:20:20:0:0 per leaflet for the synaptic vesicle membrane model and a ratio of 38:18:20:20:2:2 per leaflet for the plasma membrane model. This corresponds to 38 POPC, 18 DOPS, 20 POPE and 20 cholesterol molecules per leaflet for the synaptic vesicle membrane, and 38 POPC, 18 DOPS, 20 POPE, 20 cholesterol, 2 $PI(4,5)P_2$ (POPI25) and 2 diacylglycerol (POGL) molecules per leaflet for the plasma membrane. Relaxation and equilibration at 300 K were performed following the protocol supplied by CHARMM-GUI.[62,63] Briefly, the protocol consisted of six equilibration simulations, namely 2 x 125 ps NVT, 1 x 125 ps NPT and 3 x 500 ps NPT, gradually releasing the restraints on the lipids. Finally, a 10 ns unrestrained simulation in the NPT ensemble using the Nosé-Hoover thermostat and the Parrinello-Rahman barostat was performed. The last frame of this simulation was used for assembling the protein-lipid system.

Simulation of C2A and C2B membrane interactions

Equilibrated membrane structures were centred in the *xy*-plane and the equilibrated protein was placed at a 4 Å distance above the plane using VMD.[64] For each protein-membrane combination, three input structures with the C2 domains oriented at an angle of 0°, 30° and 60° between the *z*-axis and a vector through the main axis of the C2 domain (from the centre of mass of the protein to the centre of mass of residue 172 of C2A and residue 305 of C2B, respectively) with the Ca^{2+} binding loops facing towards the membrane were generated. Subsequently, energy minimization and a six-step equilibration protocol as described for initial equilibration of the membranes (see above) were performed. For production in the NPT ensemble the Nosé-Hoover thermostat (300K; 1 ps coupling constant for water and ions; 2.5 ps for protein and lipids) and the Parinello-Rahman barostat (semi-isotropic; 5 ps time constant). Simulations were computed until >1500 ns simulation time were accumulated.

Analysis of structural dynamics

Calculation of root-mean-square deviation and fluctuation

Root-mean-square deviation with respect to the first frame of the simulation and root-mean-square fluctuation with respect to an average structure of the last 800 ns of each simulation were calculated using functions provided by MDAnalysis.[67]

Contact angles

Trajectories of 1 ns time step per frame were generated with GROMACS and loaded into MDAnalysis.[67] The membrane interaction angle of the C2 domains was calculated between the z-axis and a vector through the main axis of the C2 domains (C2A: Tyr151 to Pro179, and C2B: Tyr282 to Pro 310). Median contact angles during the last 800 ns of the simulation were calculated for each simulation. Mean and standard deviation were reported.

Protein-lipid contacts

The most proximal lipid molecules for every amino acid residue were determined for every frame of each simulation using a k-dimensional tree[73] initialized with the centre-of-mass positions of the lipid atoms and queried with the centre-of-mass positions of the protein atoms. The resulting list was filtered and only nearest neighbours with a distance <2.6 Å were retained. Duplicate contacts (i.e. the same combination of amino acid residue number and lipid molecule) were removed. Contacts that were not observed continuously for a time span of at least 10 ns were not considered. Contact counts were summed for every simulation and averaged across the three simulations. For comparison between simulations, counts for each lipid were divided by the sum of counts of all lipids in a simulation and by the relative percentage of this lipid in the membrane lipid composition. Structural representations of lipid contacts were generated using the raw lipid contacts by mapping these values to the B-factor column of a PDB file. Visualization was performed in open source PyMol (https://github.com/schrodinger/pymol-open-source).

Local membrane reorganisation

To determine effects on local membrane organisation, all atoms were translated for each frame of the last 800 ns simulation time so that (i) the C2 domains were centred laterally and (ii) the membrane leaflets were located entirely within the simulation box. For control simulations without the proteins, only membrane leaflets were translated inside the box. Lipid atoms were wrapped inside the box for both sets of simulations. Surface positions of the phosphor atoms of the phospholipids were calculated using the membrane curvature tool of MDAnalysis (https://github.com/MDAnalysis/membrane-curvature) specifying binning into 8 x 8 bins (approx. 9 x 9 Å per bin).

Visualisation of domain insertion

Atoms for every frame of all simulations were translated so that (i) the C2 domains were centred laterally and (ii) the membrane leaflets were located completely within the simulation box. Positions of phosphor atoms of the phospholipids were calculated and visualized

using the Membrane Curvature tool implemented in MDAnalysis specifying binning into 8 x 8 bins. For comparison between simulations, surface positions were reported relative to the lowest phosphor atom coordinate.

QUANTIFICATION AND STATISTICAL ANALYSIS

Native MS measurements in the absence/presence of Ca^{2+} were performed in duplicates. All other measurements and experiments were performed at least three times. Representative results are shown. MD simulations were performed three times with different starting orientation. Relevant statistical information is provided in the figure legends and in the corresponding method details.